



# Handheld and portable X-ray Fluorescence spectrometers: Conceptual design, Qualitative analysis, advantages and limitations

**Andreas Karydas**

*Institute of Nuclear and Particle Physics  
NCSR "Demokritos"  
Agia Paraskevi  
Athens, Greece*

[karydas@inp.demokritos.gr](mailto:karydas@inp.demokritos.gr)

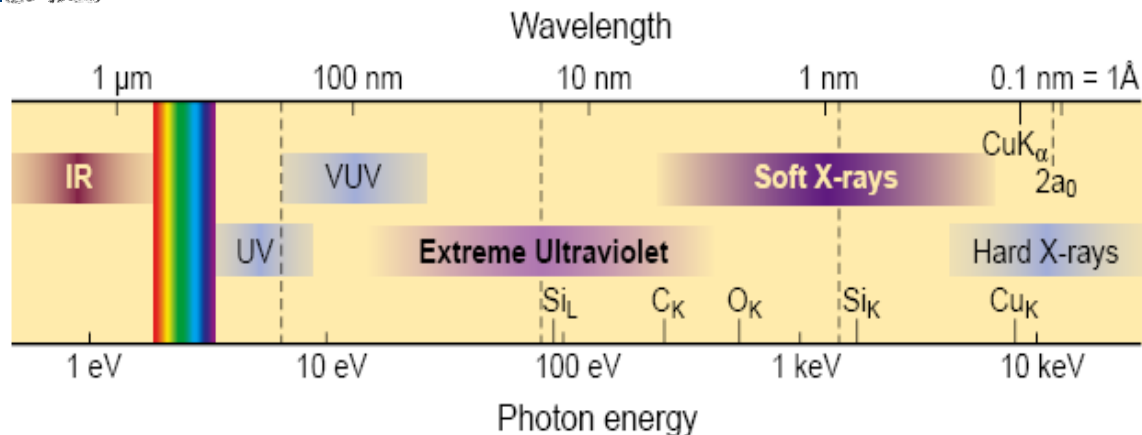


# Outline

- Principles of XRF analysis
- Qualitative analysis
- X-ray instrumentation: Sources, Detectors, optics
- Optimization of Hand-held/portable XRF analysis



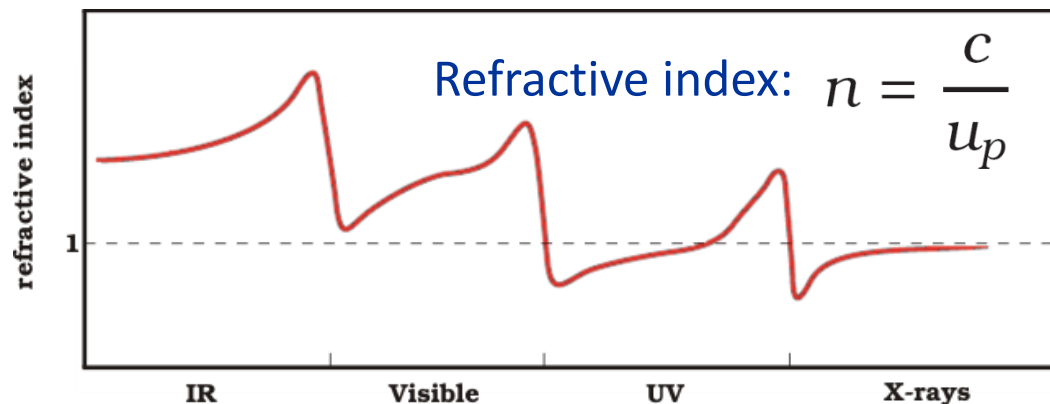
# Basic properties of X-rays



X-Ray Regime of Energies -  
Wavelengths:  
0.2 keV - 98 keV  
→ 40 Å - 0.13 Å

$$E(\text{keV}) = \frac{12.398}{\lambda(\text{Å})}$$

E: energy (keV)  
λ : wavelength (Å)

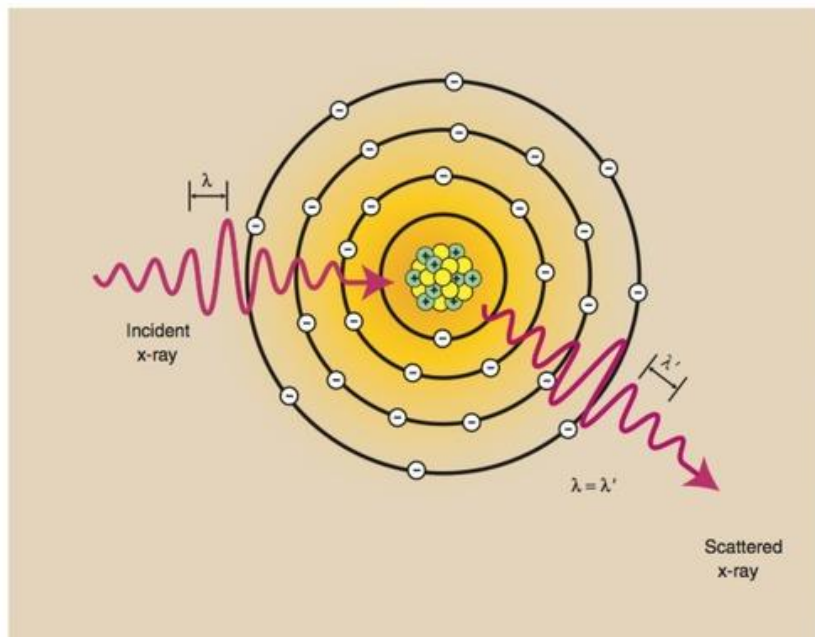


$$n = 1 - \delta + i\beta$$

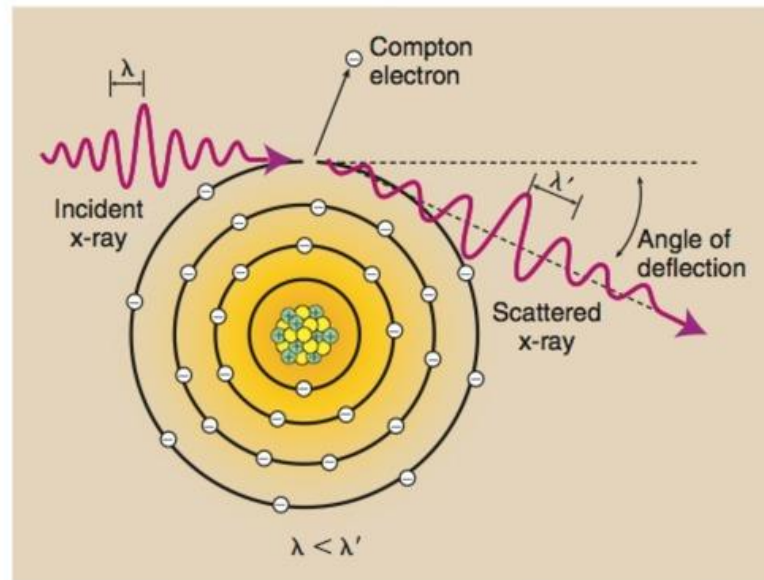
→ phase term  
→ attenuation term



# X-ray Scattering Interactions with atoms



$E_i = E_0$  : Coherent (Rayleigh),  
it occurs mostly with inner-shell  
atomic electrons

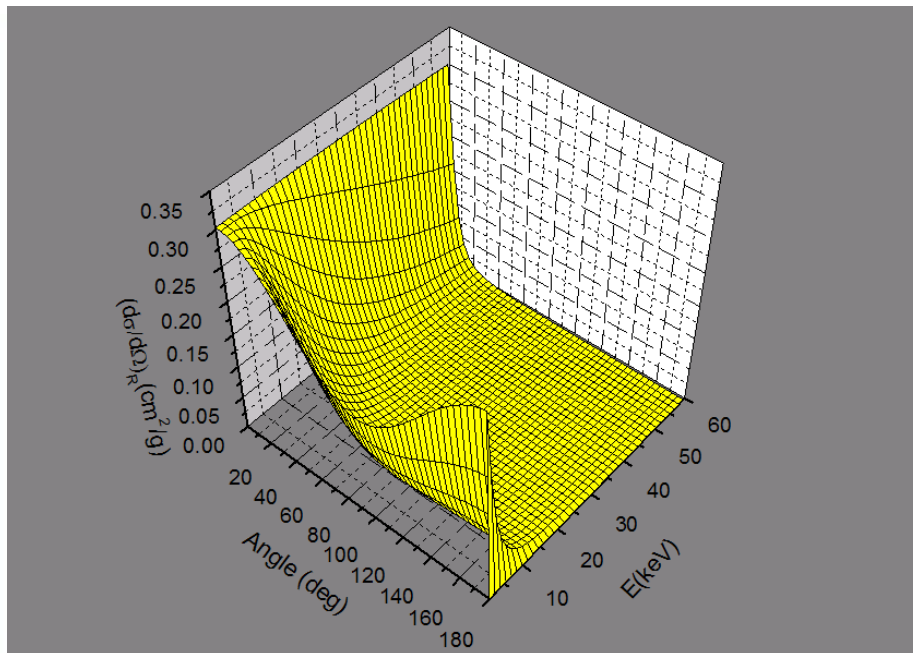


$E_i < E_0$  : Incoherent (Compton),  
it occurs mostly with outer, less  
bound electrons

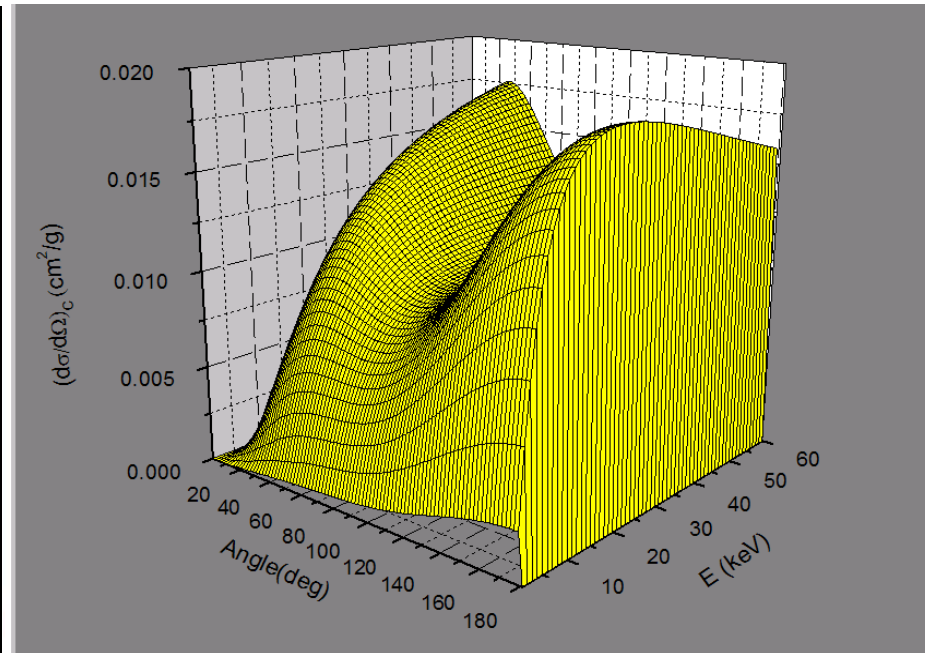
$E_0 \gg$  Binding Energy



# X-ray Scattering Interactions with atoms



$E_i = E_0$  : Coherent (Rayleigh),  
it occurs mostly with inner-shell  
atomic electrons

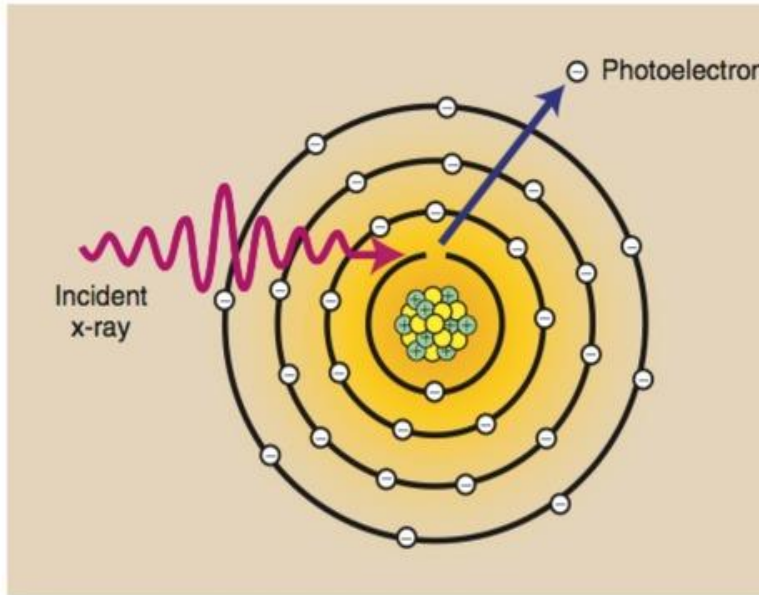


$E_i < E_0$  : Incoherent (Compton),  
it occurs mostly with outer, less  
bound electrons

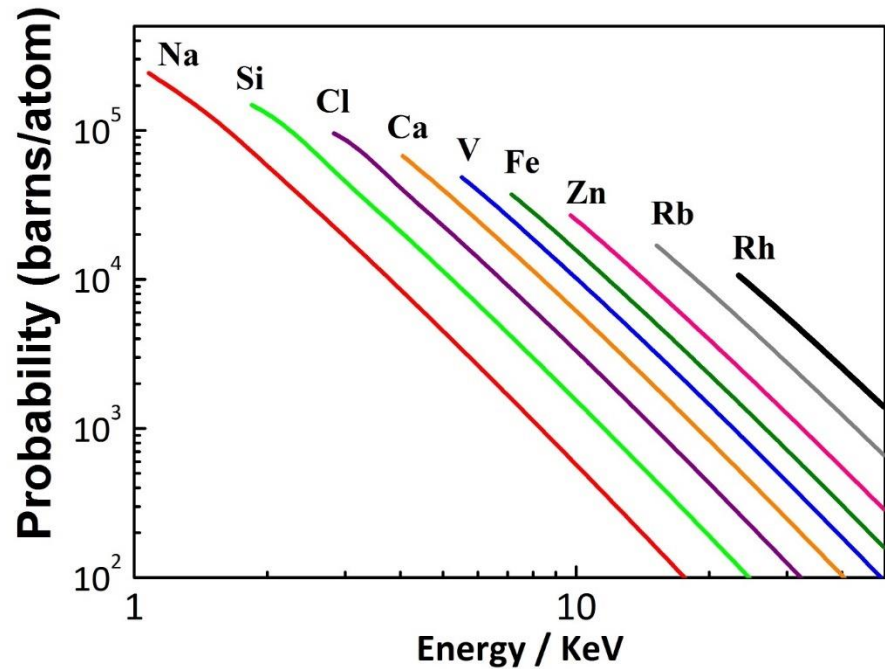
$E_0 \gg$  Binding Energy



# Photoelectric interaction



**Basic Condition:  $E_0 \geq$  Binding energy of the inner-shell electron**



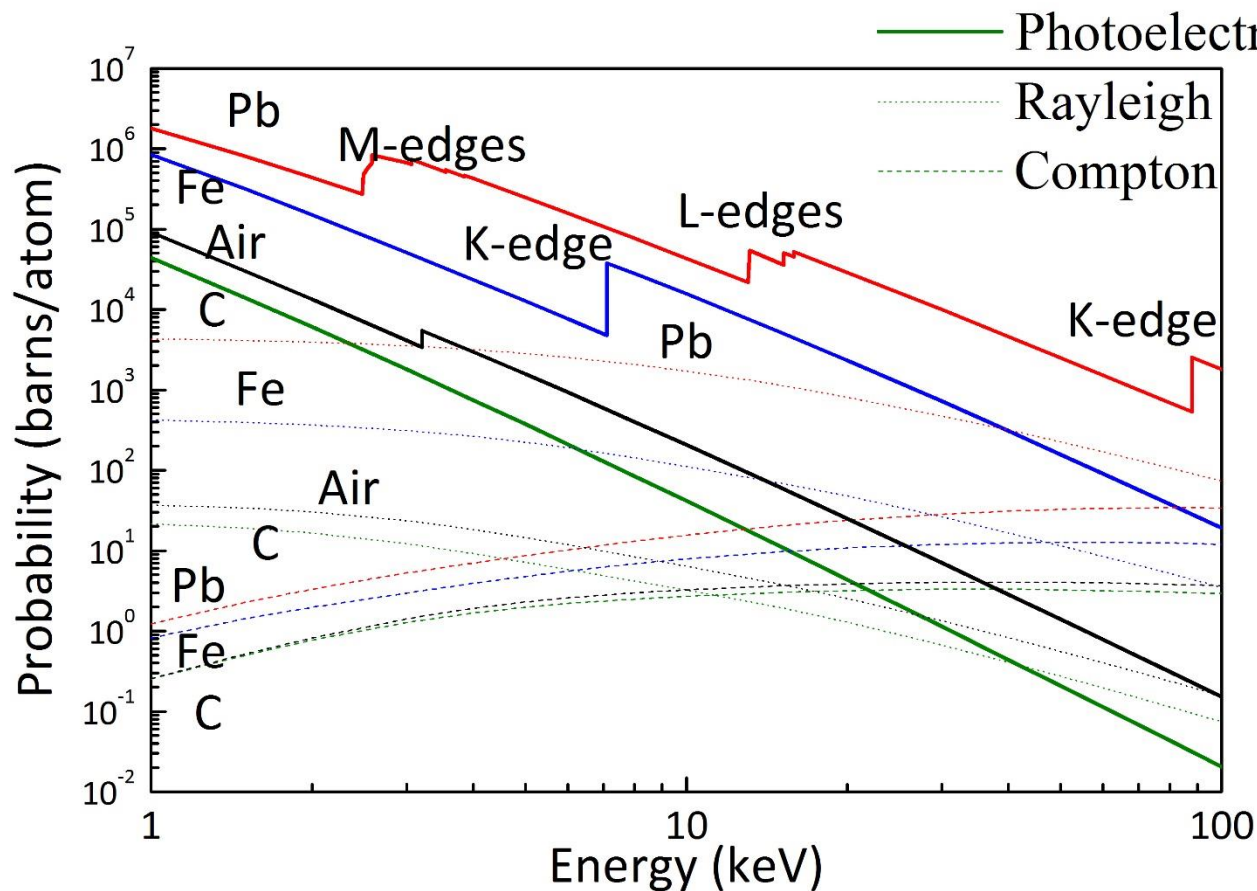
Photoelectric cross section:

$$\tau \sim E^{-3.5}$$

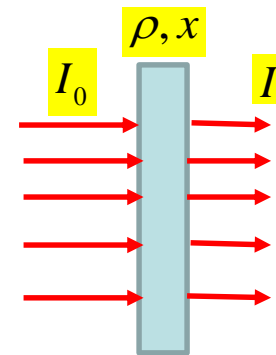
$$\tau \sim Z^3 \text{ to } 4$$



# X-rays interactions with matter



Beer-Lambert law



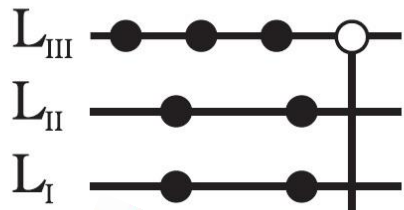
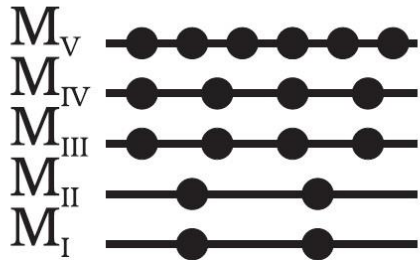
$$I = I_0 \cdot e^{-(\tau + \sigma_R + \sigma_C) \cdot \rho \cdot x}$$

Ratio photo./scat.  
 $\approx$  **1000 - 10000**

**Photoelectric is the dominant process**



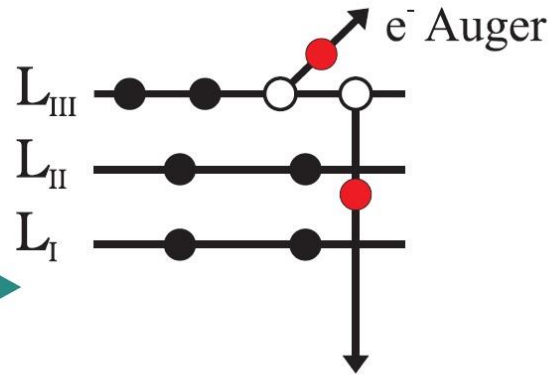
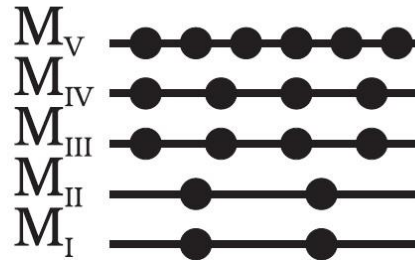
# Atomic Relaxation



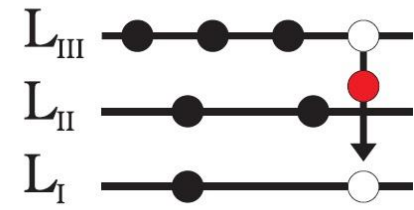
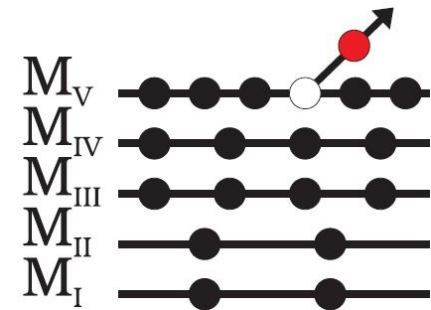
$h\nu$

$K\alpha_1$

K  
Φθορισμός  $K\alpha_1$



K  
Auger  $KL_{III}L_{III}$

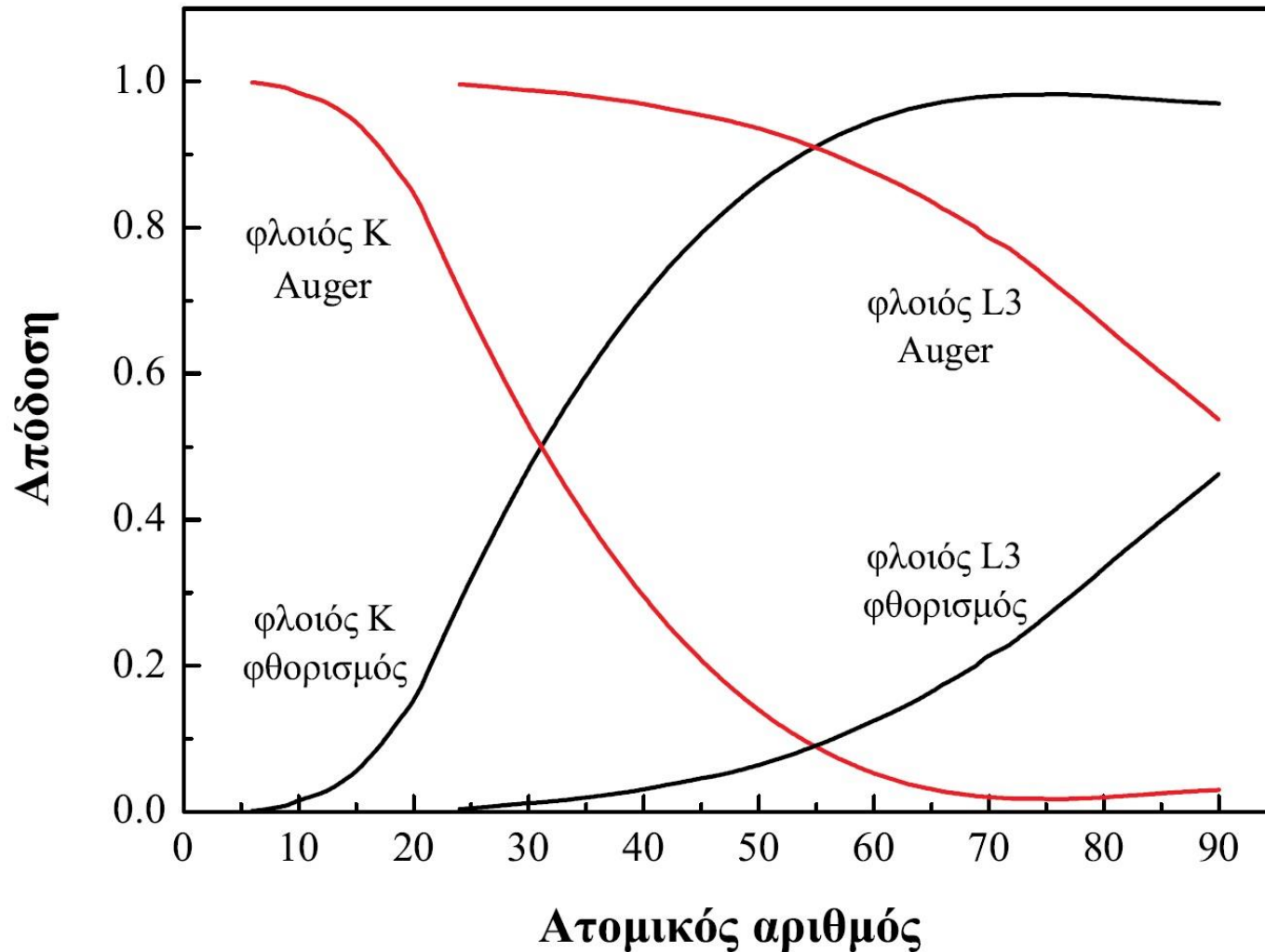


K  
Coster Kronig  $L_I L_{III} M_V$





# Fluorescence probability

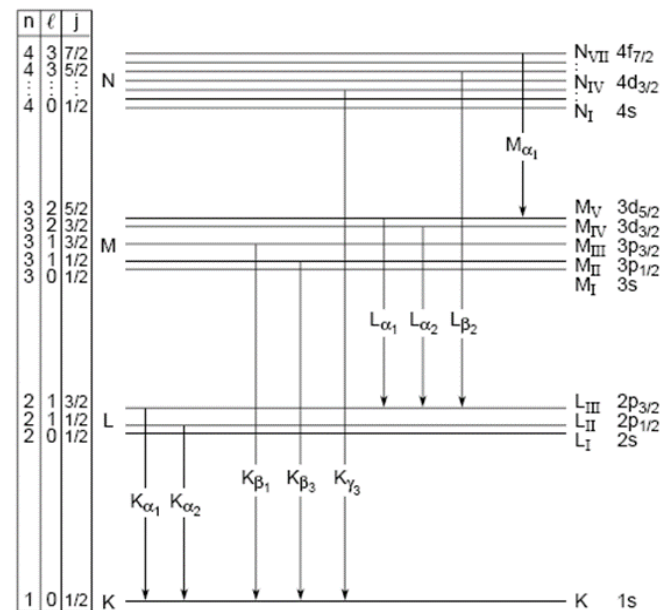


Example: The fluorescence probability for Si is almost 5%, only 5 holes decay through emission of fluorescence K radiation over 100 primary ionizations



# Emission of element 'characteristic' x-rays

The emission of characteristic X-ray lines follows allowed electronic transitions between specific subshells



**Siegbahn/IUPAC**

**notation:**

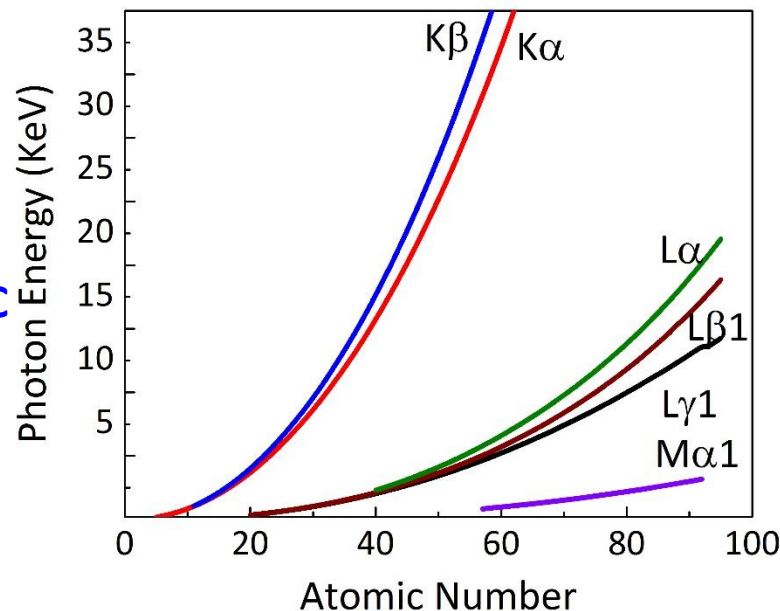
**K<sub>α</sub>**: K-L2+K-L3

**K<sub>β</sub>**: K-M2+K-M3

**L<sub>α</sub>**: L3-M4+L3-M5

**L<sub>β1</sub>**: L2-M4

**L<sub>β2</sub>**: L3-N5



Moseley law:

$$E_{ij} = k_{ij} \cdot (Z - \sigma_i)^2$$

**L<sub>III</sub> to K shell:**  $E_{K\alpha1} = U_K - U_{LIII}$

Unique set of emission energies

for each element

X-ray spectroscopy within the energy range 1-30keV offers in principle the possibility to detect all the periodic table elements through their K, L or even M series of characteristic X-ray lines



# Working principle: X-Ray Fluorescence

**Working principle:**

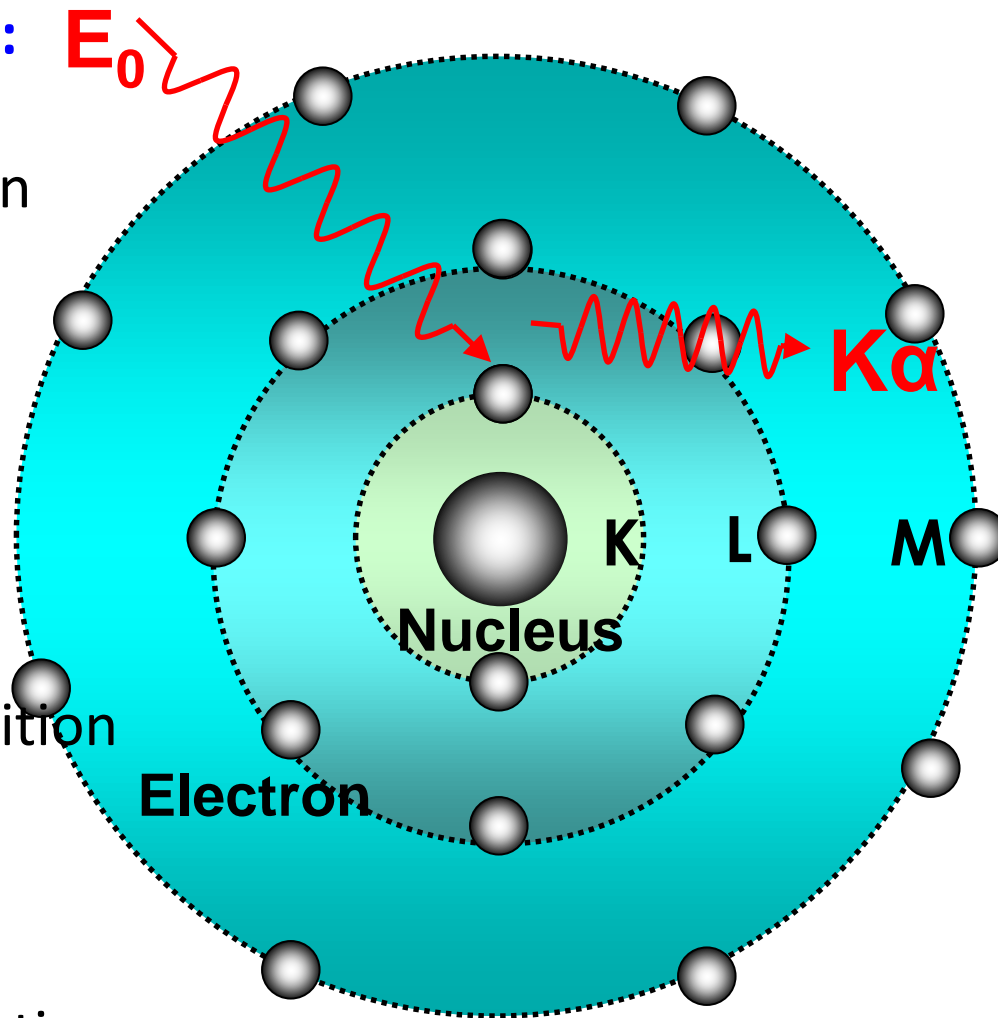
**1) Photo-ionization of atomic bound electrons**

(K, L, M)

**/Photoelectric absorption**

**2) Electronic transition and emission of element**

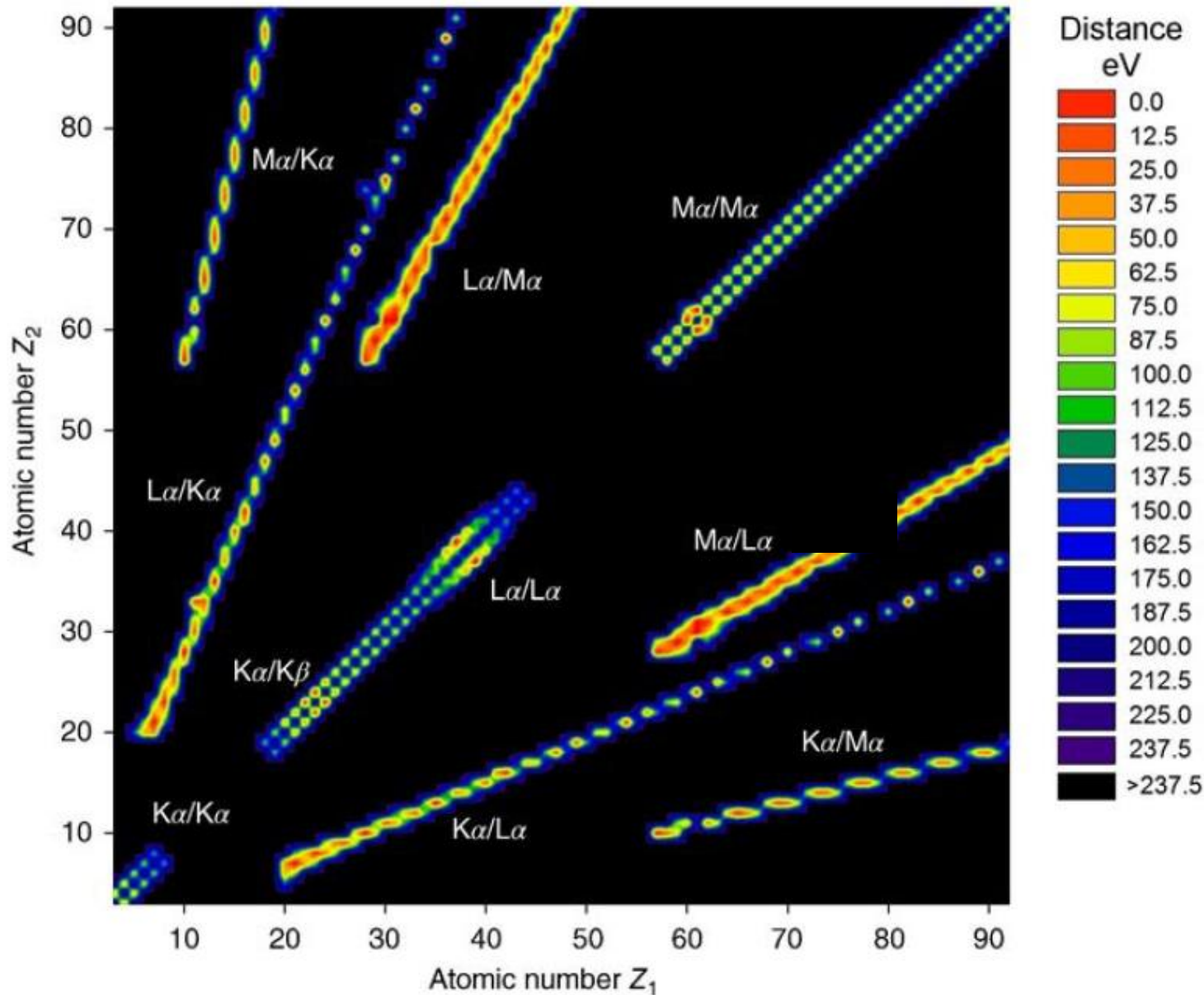
**'characteristic' fluorescence radiation**



**Incident photon Energy  $E_0$  should be adequate to ionize the atomic bound electrons**  
 **$E_0 \geq$  Inner shell binding energy**



# Spectral interferences in XRF analysis

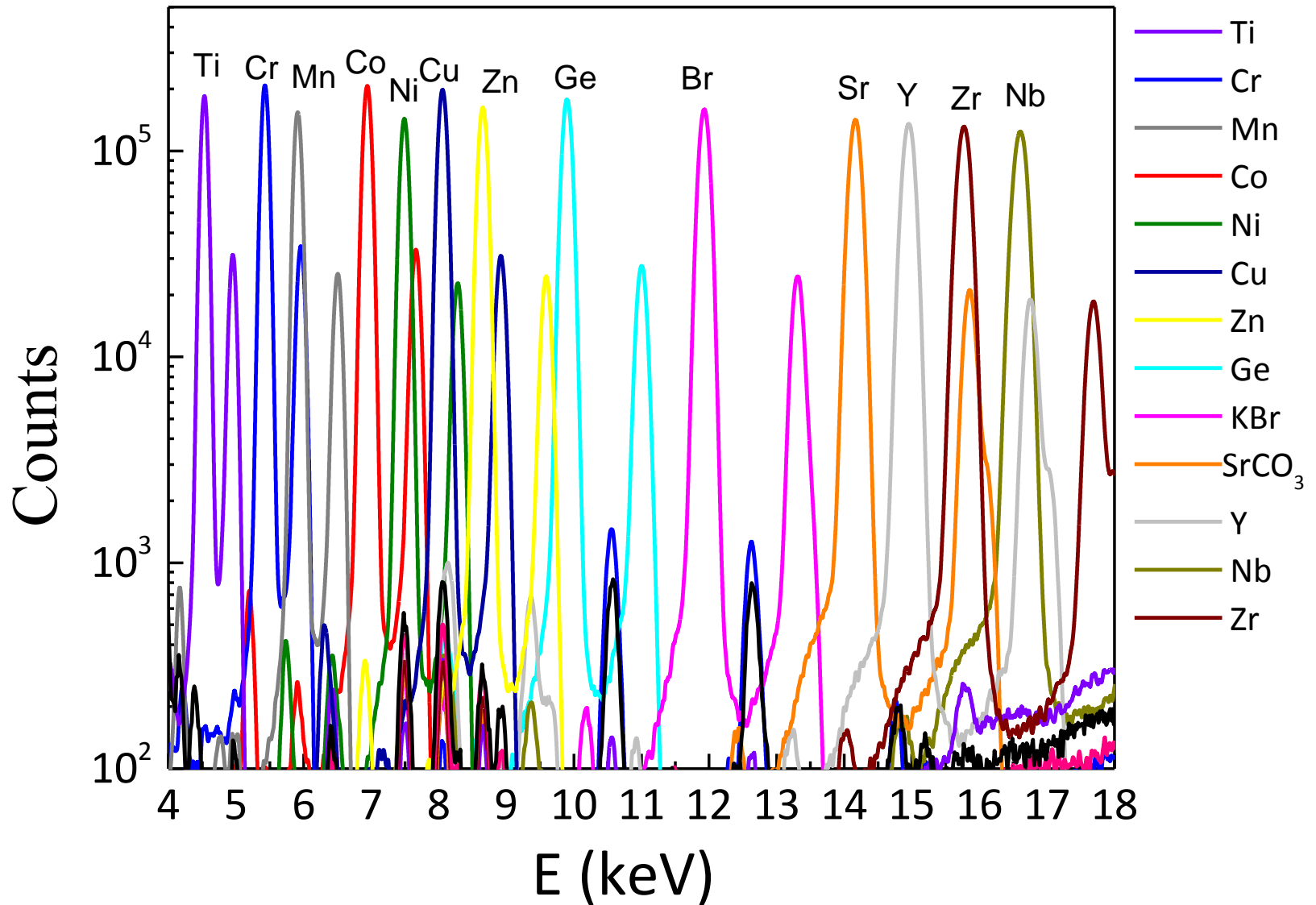


**Total-Reflection  
X-Ray  
Fluorescence  
Analysis  
and Related  
Methods,  
and Reinhold  
Klockenkämper,  
Alex von Bohlen**



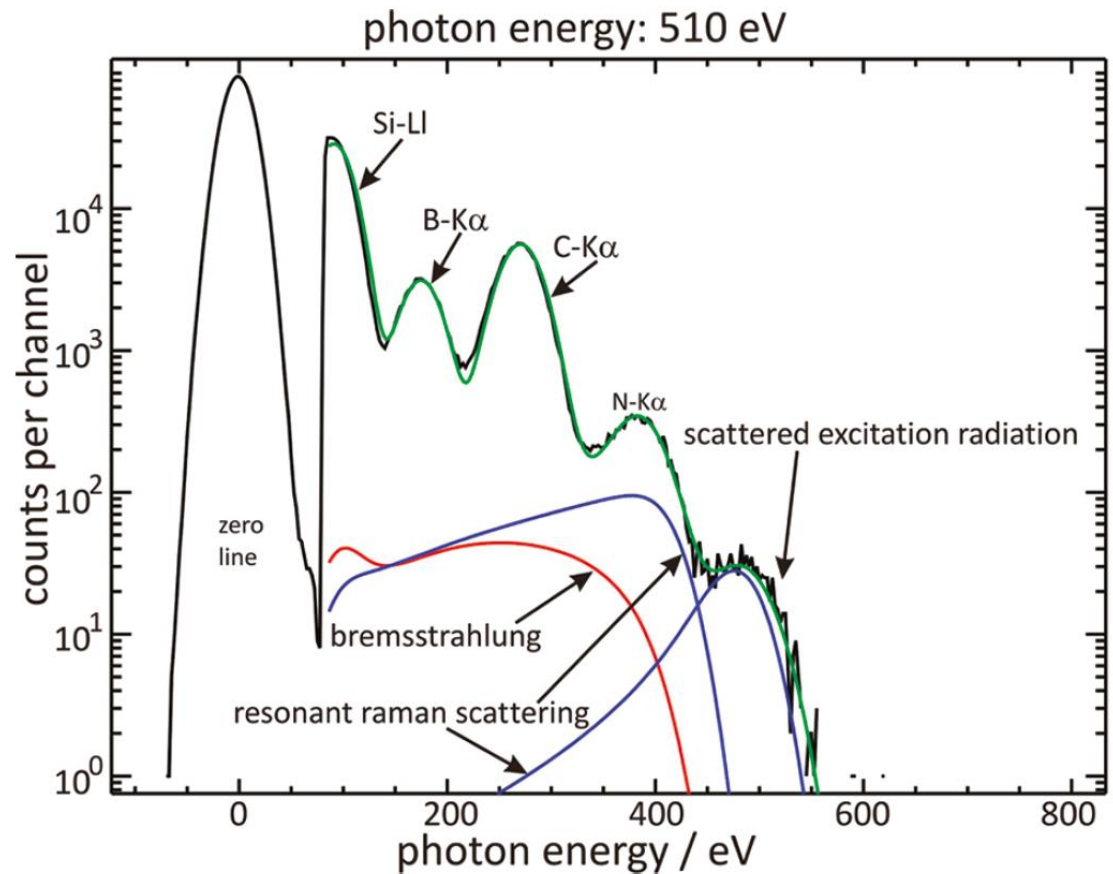
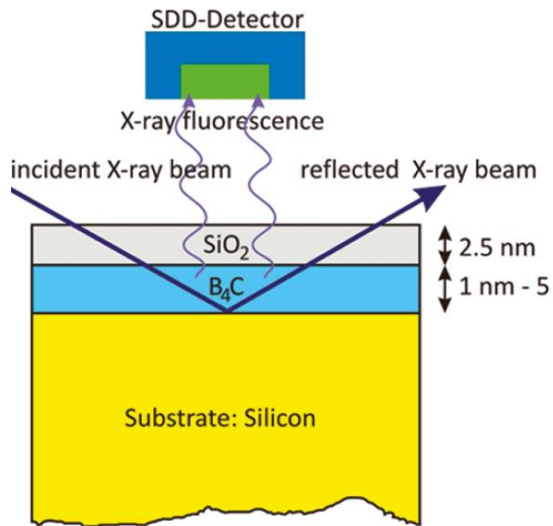
# XRF multielemental analysis: K-lines

K-Lines Spectra with Silicon Drift Detector





# Low Z XRF element analysis (down to Boron)



Unterumsberger et al., [dx.doi.org/10.1021/ac202074s](https://doi.org/10.1021/ac202074s), Anal. Chem. 2011, 83, 8623–8628

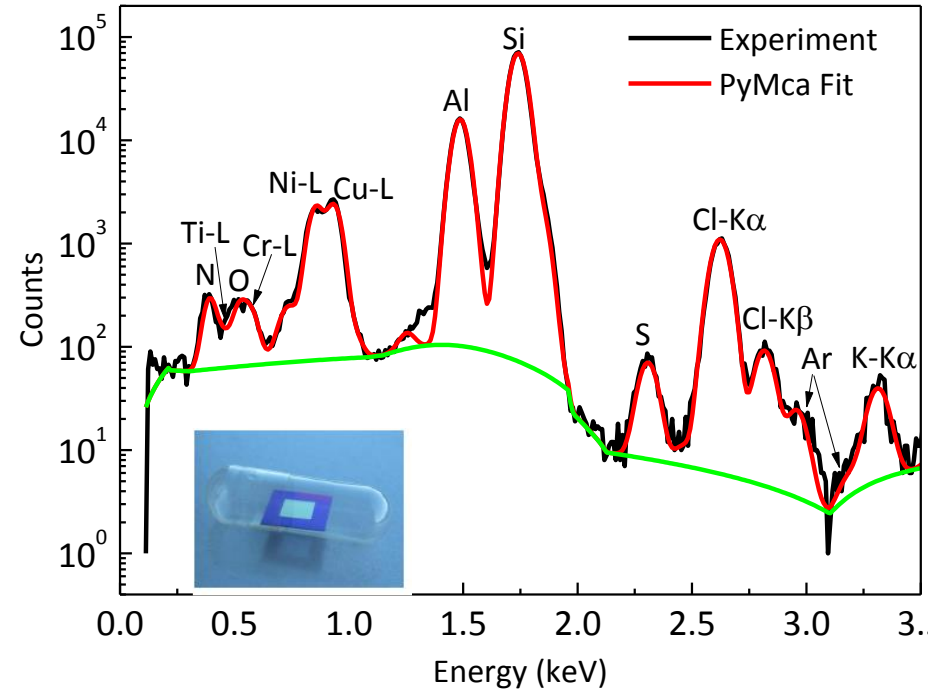
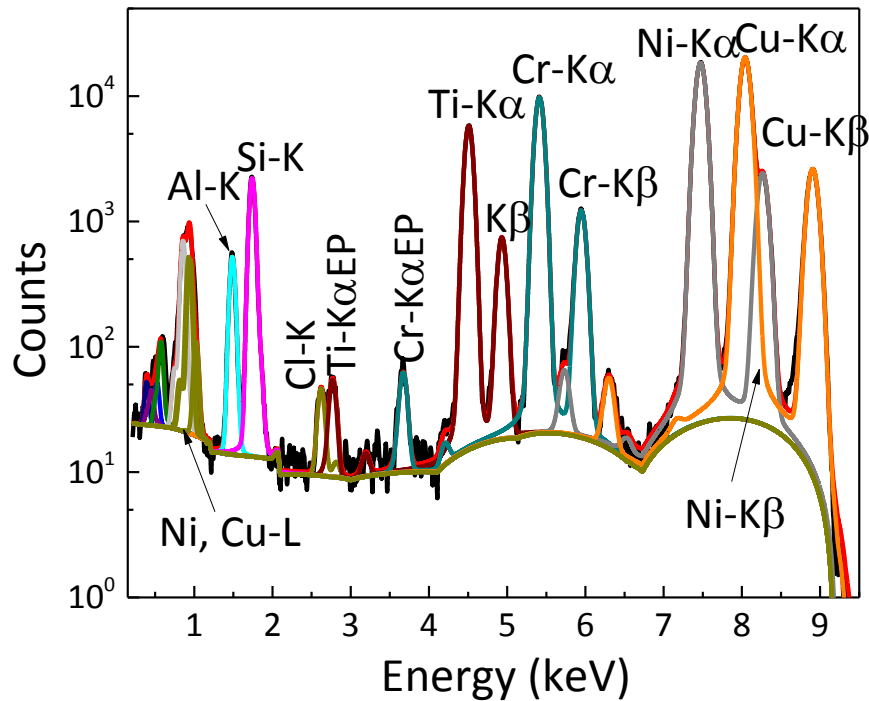




# XRF spectra of nano-layered systems

Cr/Al/Ni/Cu/Ti/ onto  $\text{Si}_3\text{N}_4$  200 nm,  
each layer about  $10 \text{ ug/cm}^2$ ,  $\sim 10\text{-}40\text{nm}$

10 keV excitation energy



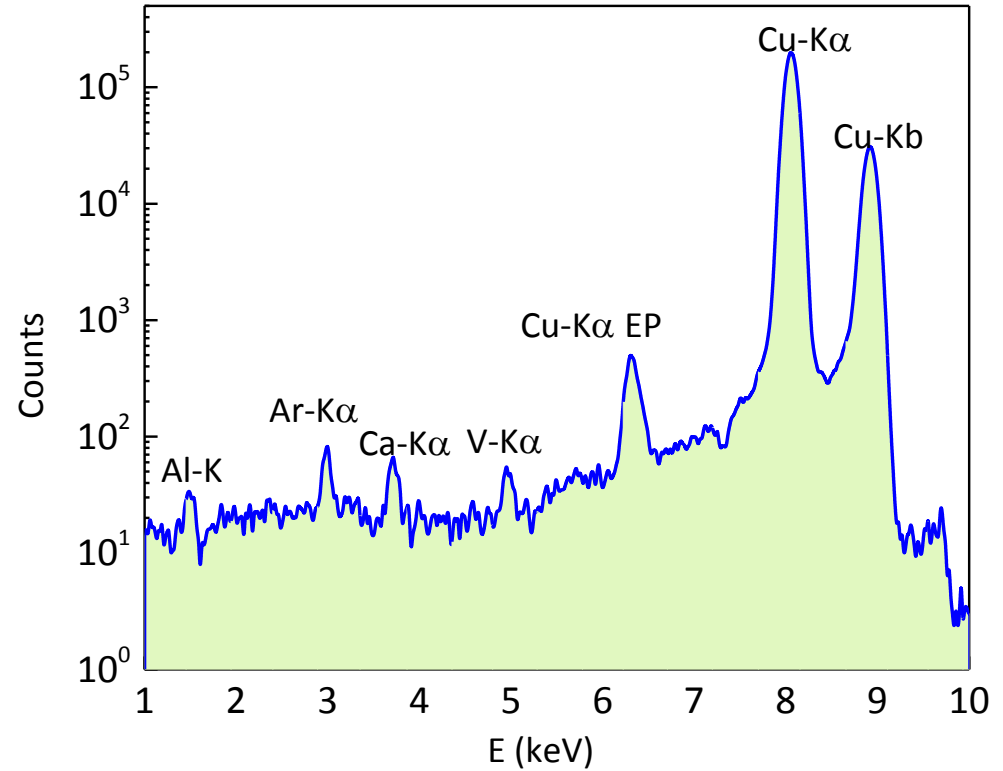
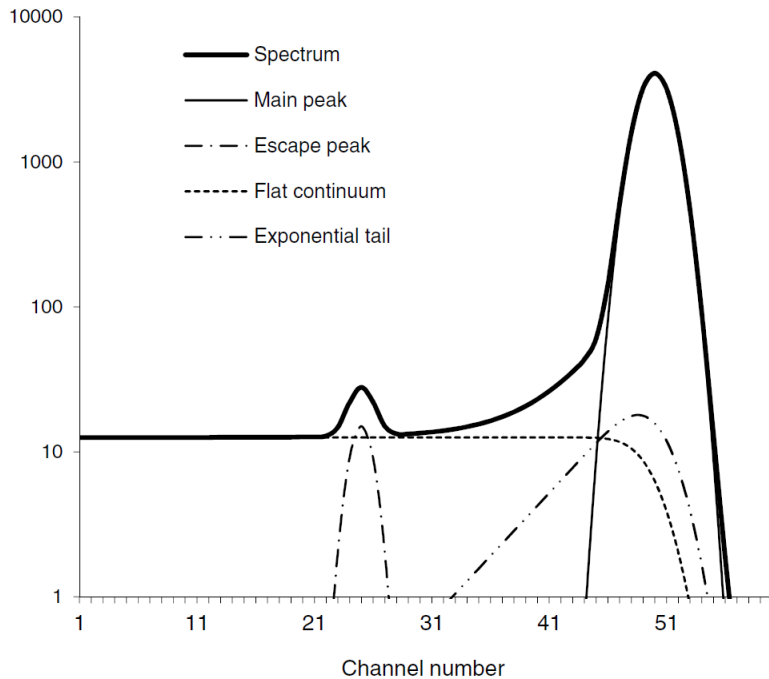
Spectra measured at Elettra Sincrotrone Trieste, XRF beamline

Karydas et al., Journal of Synchrotron Radiation, (2018). 25, 189–203





# Detector Response function



Peak shape of characteristic X-ray lines: Gaussians with tails and continuum



# XRF Analytical Sensitivity

## LoD: Limit of Detection

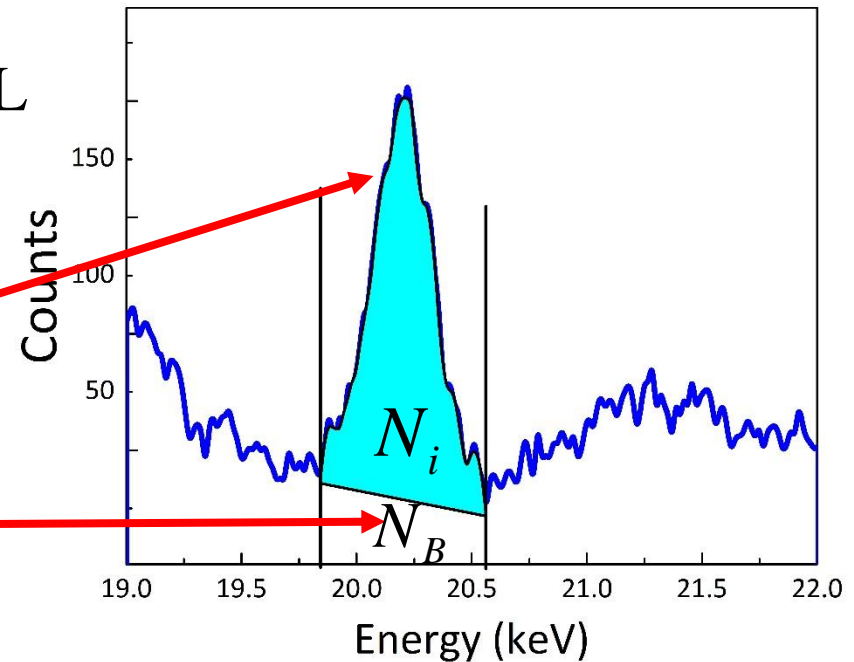
$$(LoD)_i \approx 3 \cdot c_i \cdot \frac{\sigma_i}{N_i} \quad (95\%) \text{ CL}$$

$$\sigma_i \approx \sqrt{N_B}$$

$I_i$  Fluorescent intensity (cps)

$I_B$  Background intensity (cps)

$c_i$  Analyte concentration



$$(LoD)_i \approx 3 \cdot \frac{\sqrt{I_B / t}}{(I_i / c_i)} \propto \frac{\sqrt{t}}{t}$$

$$LoQ \approx 3.3 \cdot LoD$$



# XRF Information depth

Material	X-ray line	D (μm)
Bronze 95% Cu, 5% Sn	Cu-Kα	10
	Sn-Kα	32
Gold 95% Au, 4.5 % Ag, 0.5% Cu	Cu-Kα	1.4
	Au-Lα	2
	Ag-Kα	5
Egyptian Blue 20% + 80% binder	Cu-Kα	270
	Ca-Kα	37
	Si-Kα	6

The information depth depends on:

- the sample matrix composition
- analyte energy
- incident beam energy (spectrum)
- geometry (incident/outgoing angles)

Critical thickness

$$D = \frac{1}{\rho \cdot \mu_T(E_i)}$$

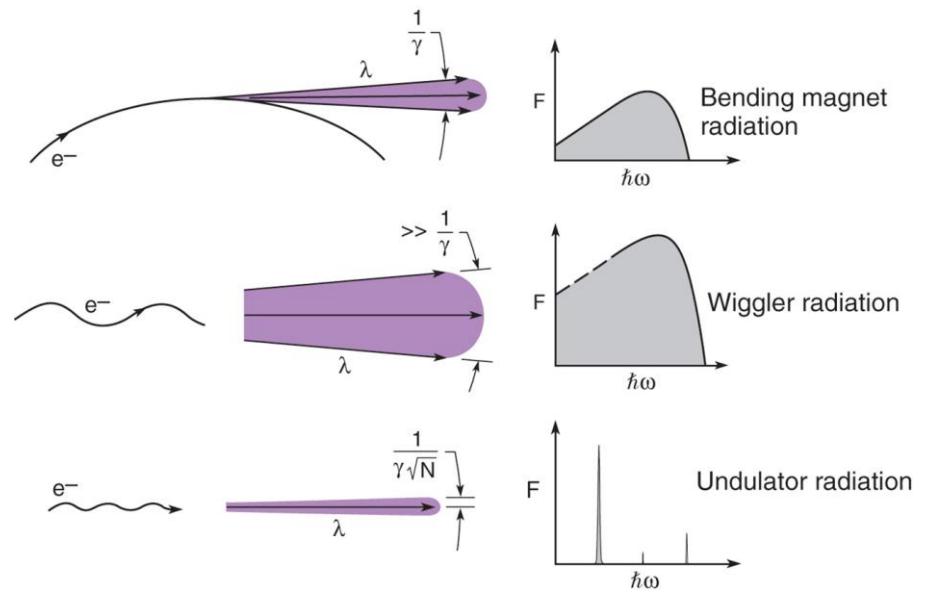
$$\mu_T(E_o, E_i) = \mu_s(E_o) / \sin \vartheta_1 + \mu_s(E_i) / \sin \vartheta_2$$



# X-ray sources

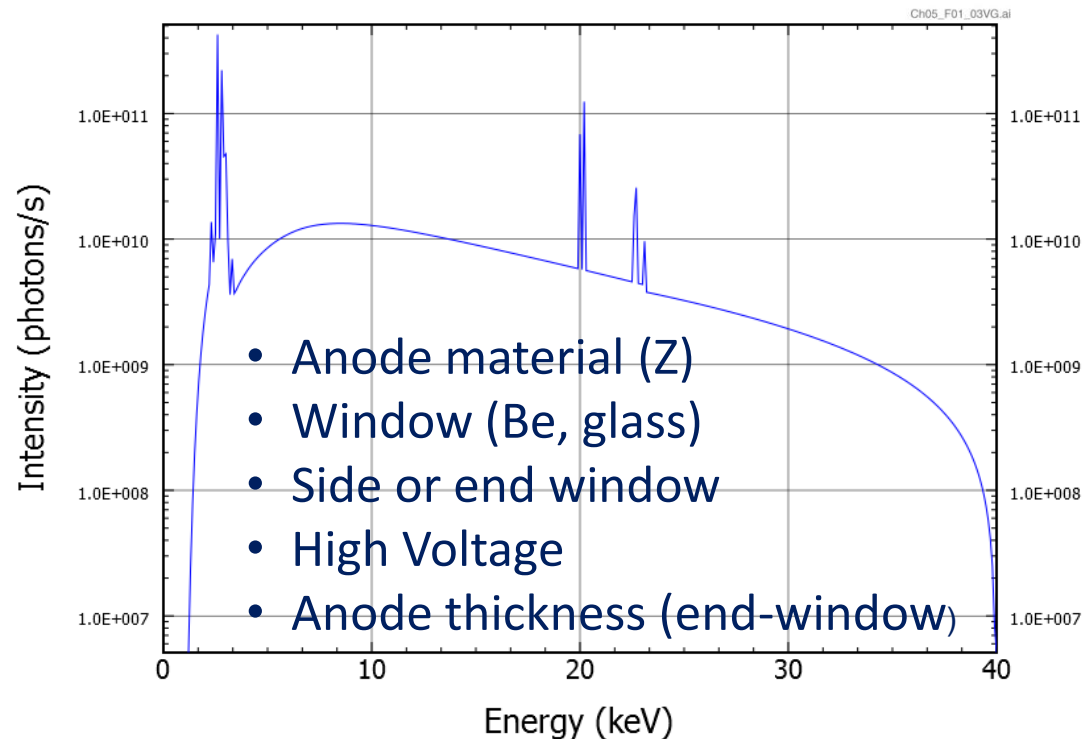
## Synchrotron radiation

High brilliance, low divergence, high polarization: Micro/Nano-XRF ( $< 1\mu\text{m}$ )



## X-ray tubes

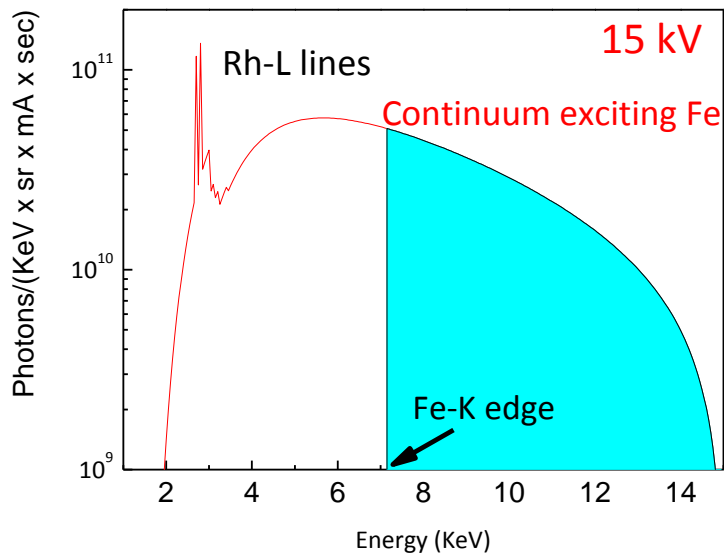
- High power ( $\sim \text{kW}$ ) diffraction x-ray tubes
- Micro focus ( $\sim 50\text{-}100\mu\text{m}$ ) anode size - Brilliance optimised (30-50 W (air cooled))
- Miniature X-ray tubes – geometry optimized (2W-12W, 50kV)



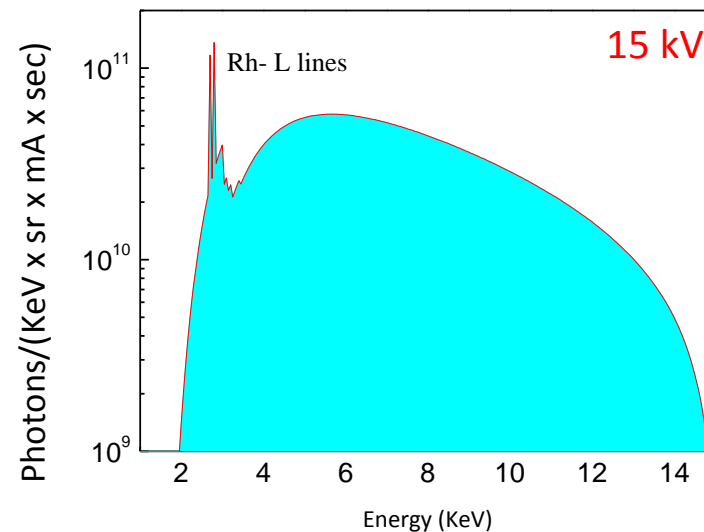


# Tube excited XRF analysis

Fe excitation

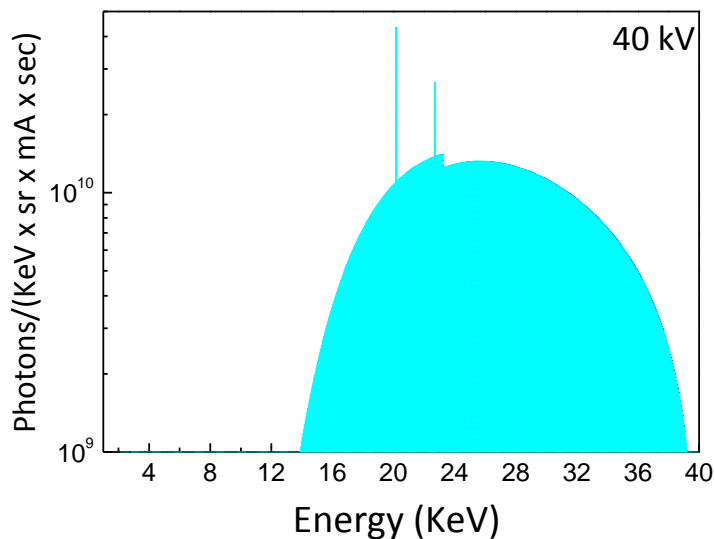


Si excitation

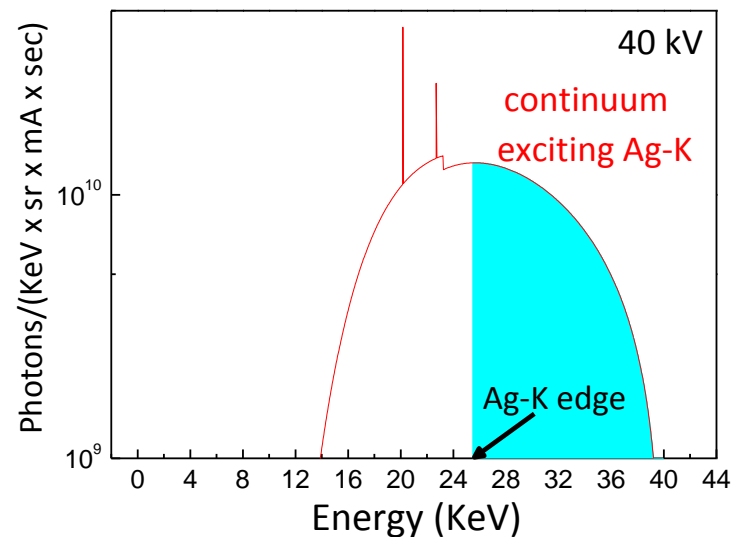


15 kV  
Unfiltered

Cu excitation



Ag excitation



40 kV  
Filtered



# XRF instrumentation: X-ray Sources-Detectors

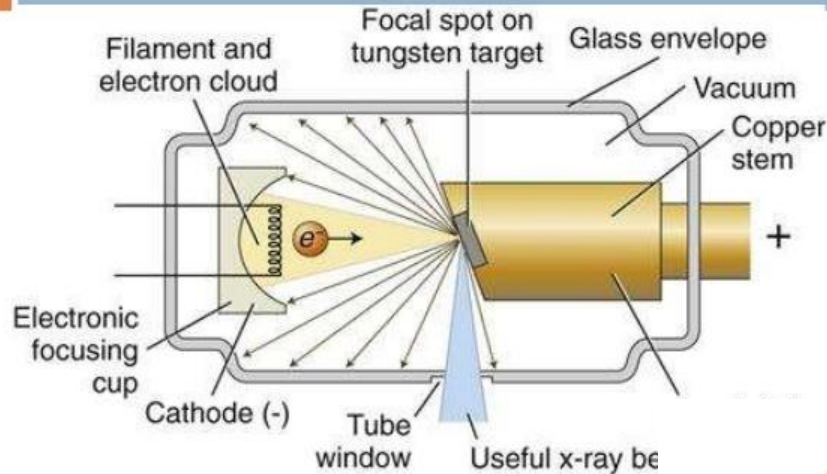
Oxford Model: XTF5011



Anode materials: Rh, Ag, Mo  
Focus spot size 50-150  $\mu\text{m}$   
Exposure < 0.5 mR/hr



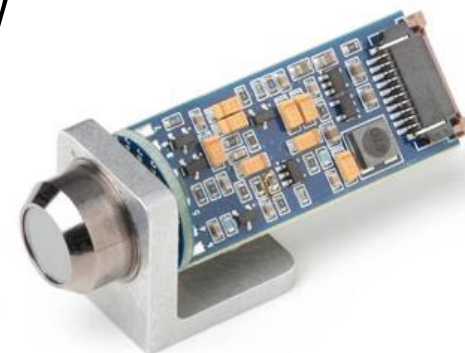
Moxtek end/side window tubes, 10W, 50kV



Newton M47, 50kV 10W  
X-ray Source, 400 grs

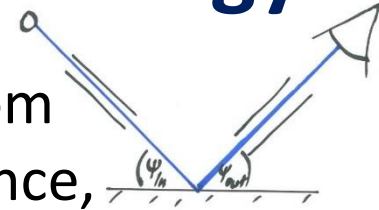


Miniature X-ray detector





# Energy Dispersive Detector's technology

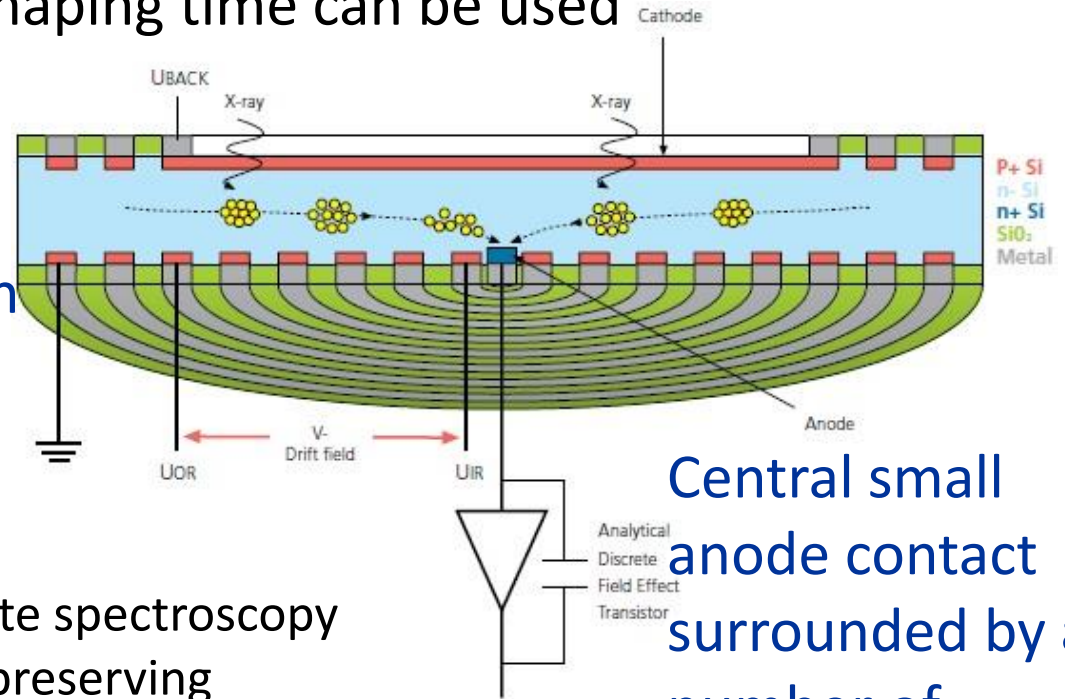


**Silicon Drift Detector - Principle:** The charge is drifted from a large area into a small read-out node with low capacitance, independent of the active area of the sensor. Thus, the serial noise decreases and shorter shaping time can be used

## Two advantages:

- 1) Faster counting is enabled
- 2) Higher leakage current can be accepted, drastically reducing the need for cooling

CUBE preamplifier supports high-rate spectroscopy in XRF mapping applications, while preserving enough energy resolution at shorter shaping times. The use of short peaking times further reduces the impact of the detector leakage current on the total noise. Room temperature operation!



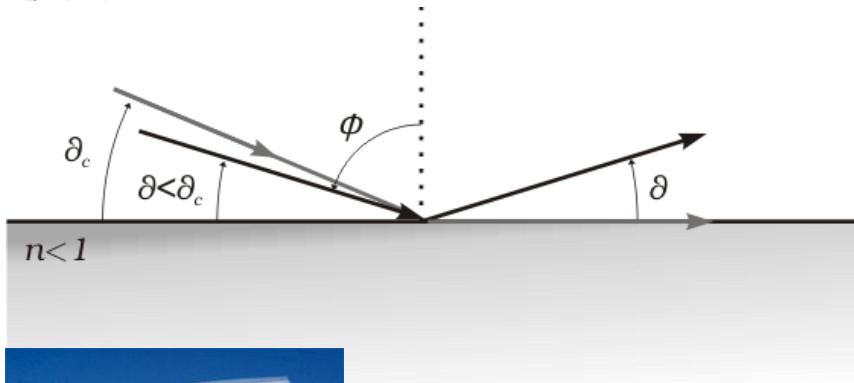
Central small anode contact surrounded by a number of concentric drift electrodes

Figure from Oxford Instruments Manual





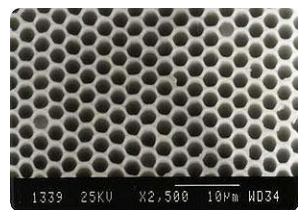
# X-ray Optics in XRF analysis: Focusing



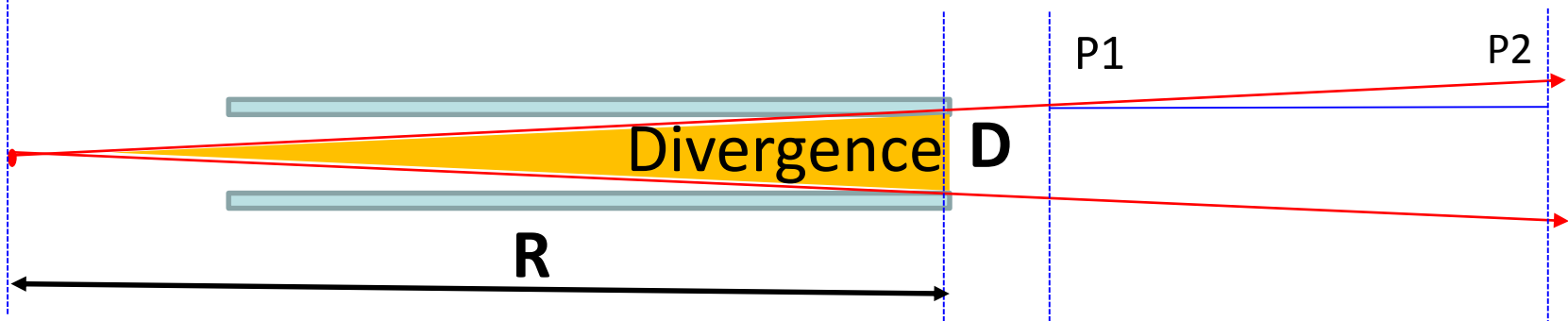
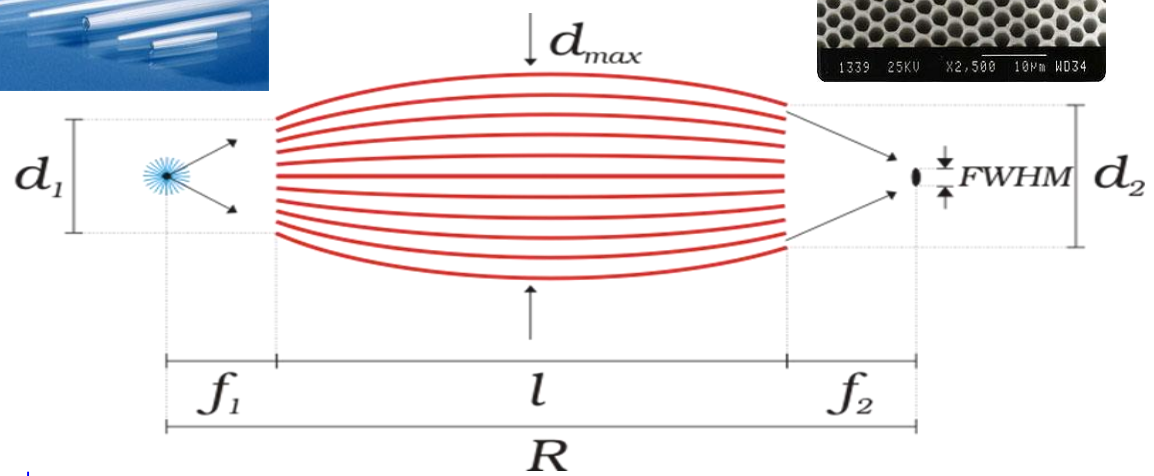
$$n \approx 1 - \delta$$

$$\vartheta_{crit} = \sqrt{2\delta}$$

$$\vartheta_{crit}(\text{degrees}) \approx \frac{1.651}{E(\text{keV})} \sqrt{\frac{Z}{A} \rho \left(\frac{\text{g}}{\text{cm}^3}\right)}$$



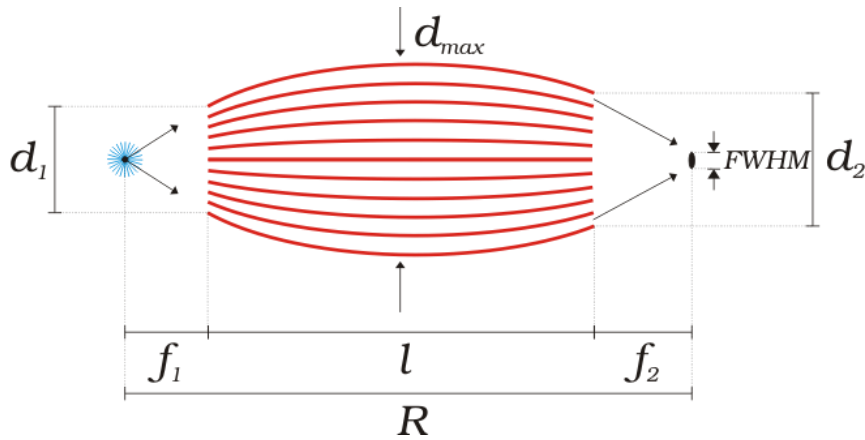
- Polycapillary full lens
- Collimator
- Curved crystals



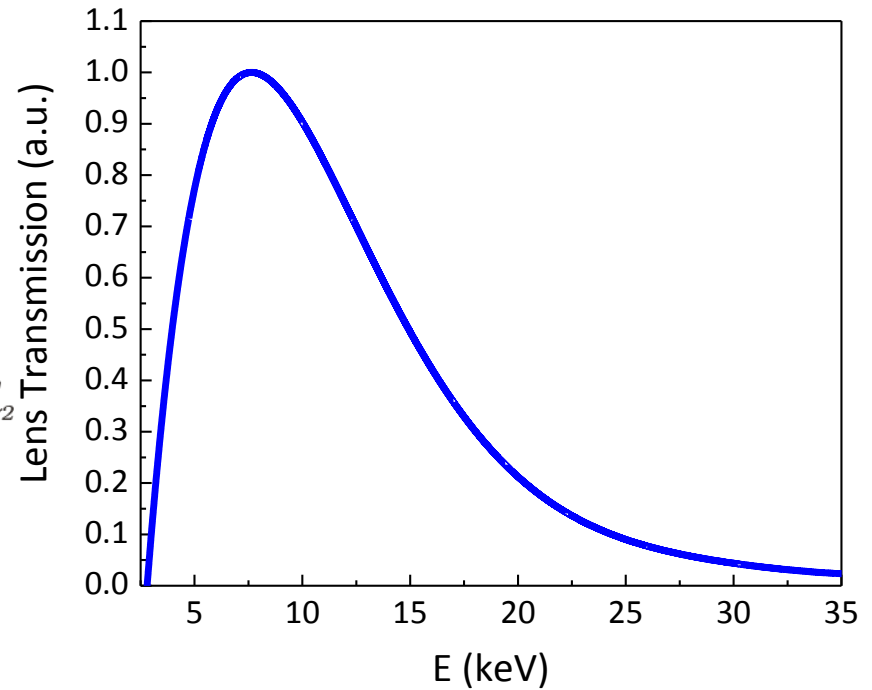


# Characteristics of Polycapillary X-ray lenses

- Spot size –FWHM (E)
- **Gain Factor – G(E)**
- Focal distance



Lens Transmission efficiency



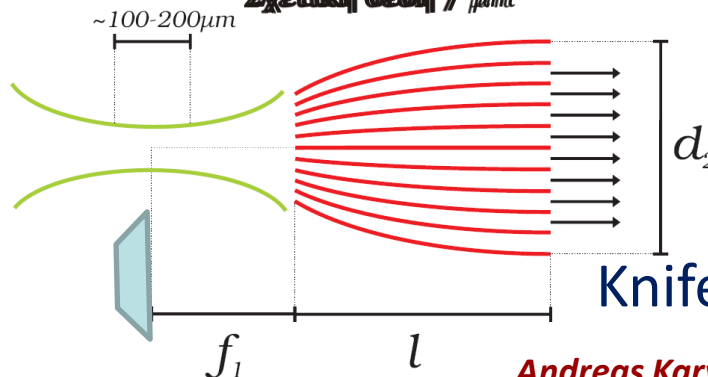
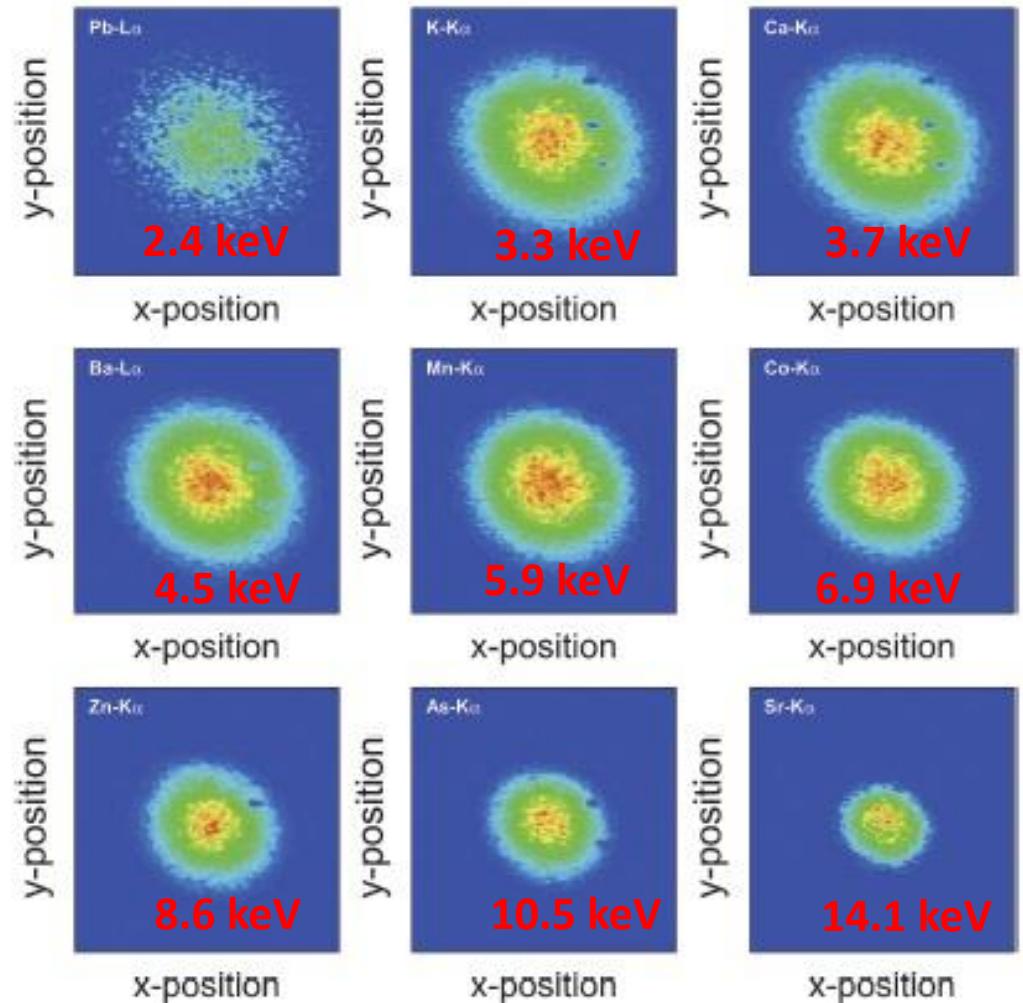
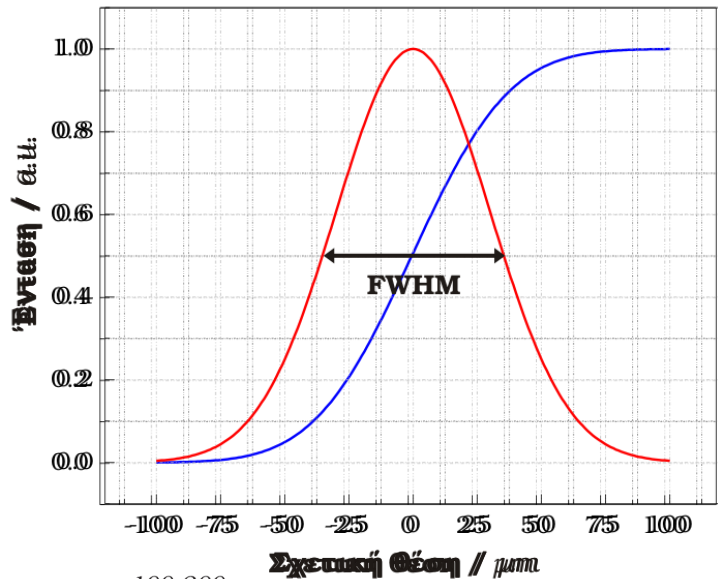
$$G(E) = \frac{\Phi_{lens}}{\Phi_{col}} = \frac{T(E) \cdot d_{in}^2 \cdot R^2}{[FWHM(E)]^2 \cdot f_1^2}$$

T(E)=transmission efficiency



# Characteristics of Polycapillary X-ray lenses

- Spot size – FWHM (E)
- Gain Factor – G(E)
- Focal distance

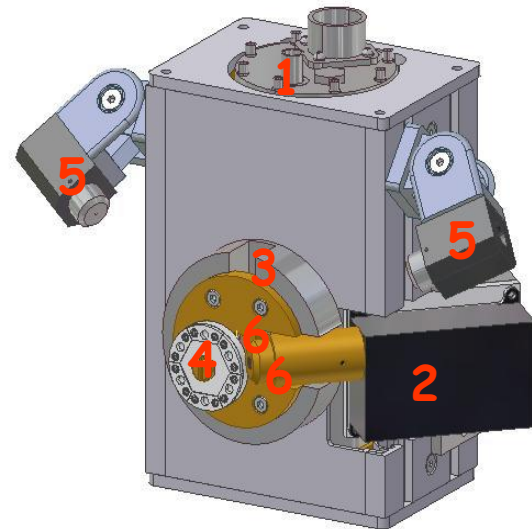
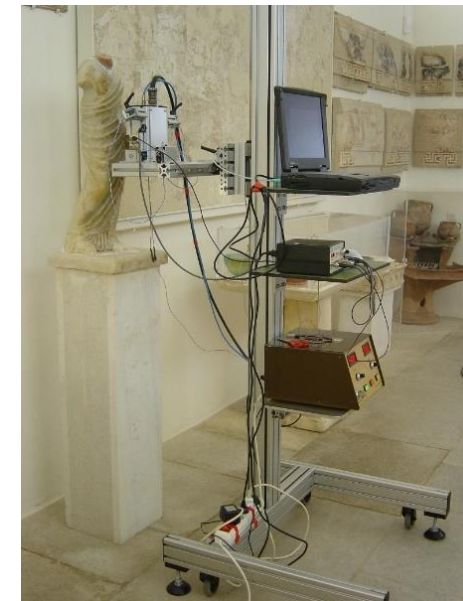
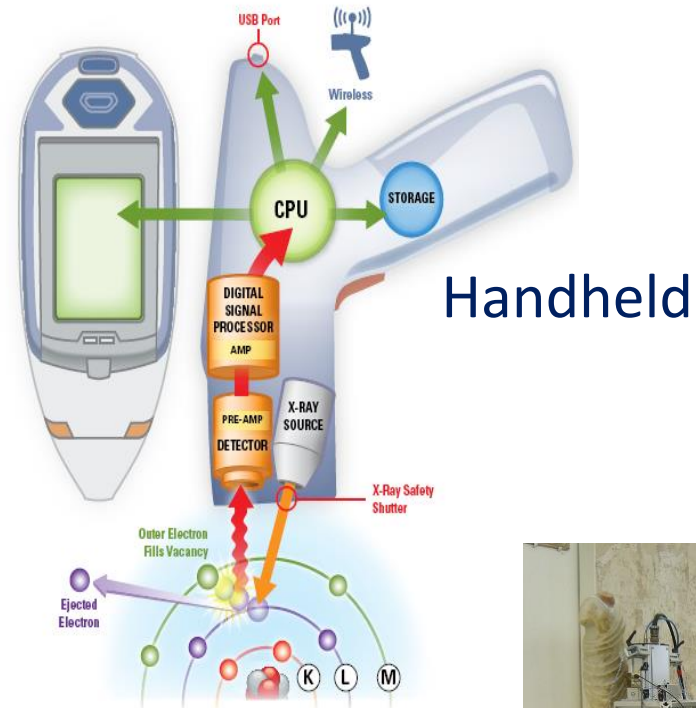
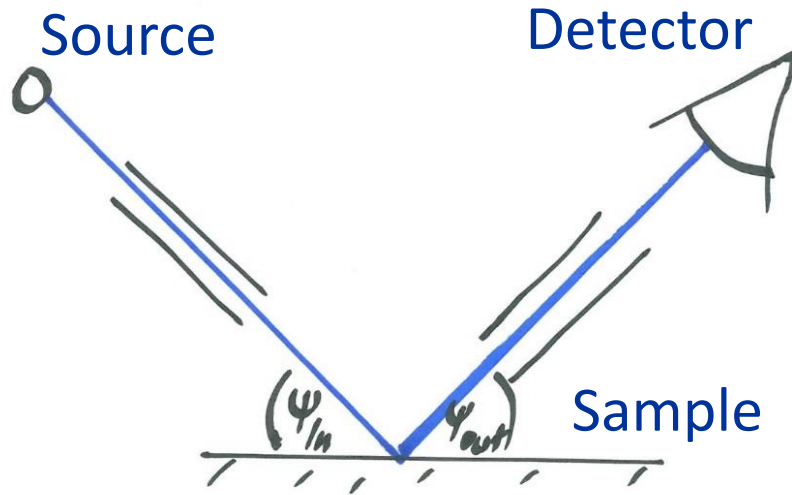


Knife edge scan

T. Wolff et al, JAAS, 2009 24 669



# Portable milli-beam spot XRF spectrometer

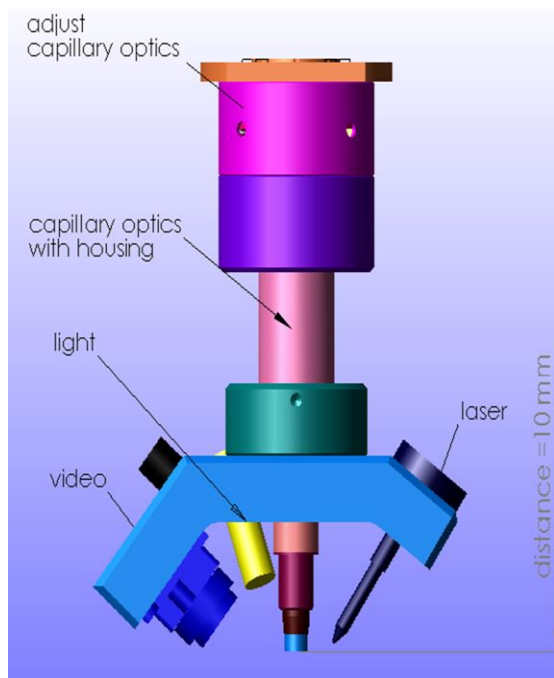


1. X-ray source,
2. X-ray detector
3. Beam shutter
4. Rotatable filter wheel
5. Lasers for sample positioning
6. Collimating parts





# Portable Micro XRF spectrometer



Customized design  
of the micro-XRF  
probe by IFG based  
on ARTAX model by  
Bruker-AXS

Headed Eagle lapis lazuli and gold  
3000 B.C. Early Bronze Age  
Archaeological Museum of Damascus October  
2007



# Fluorescence production: Selective excitation

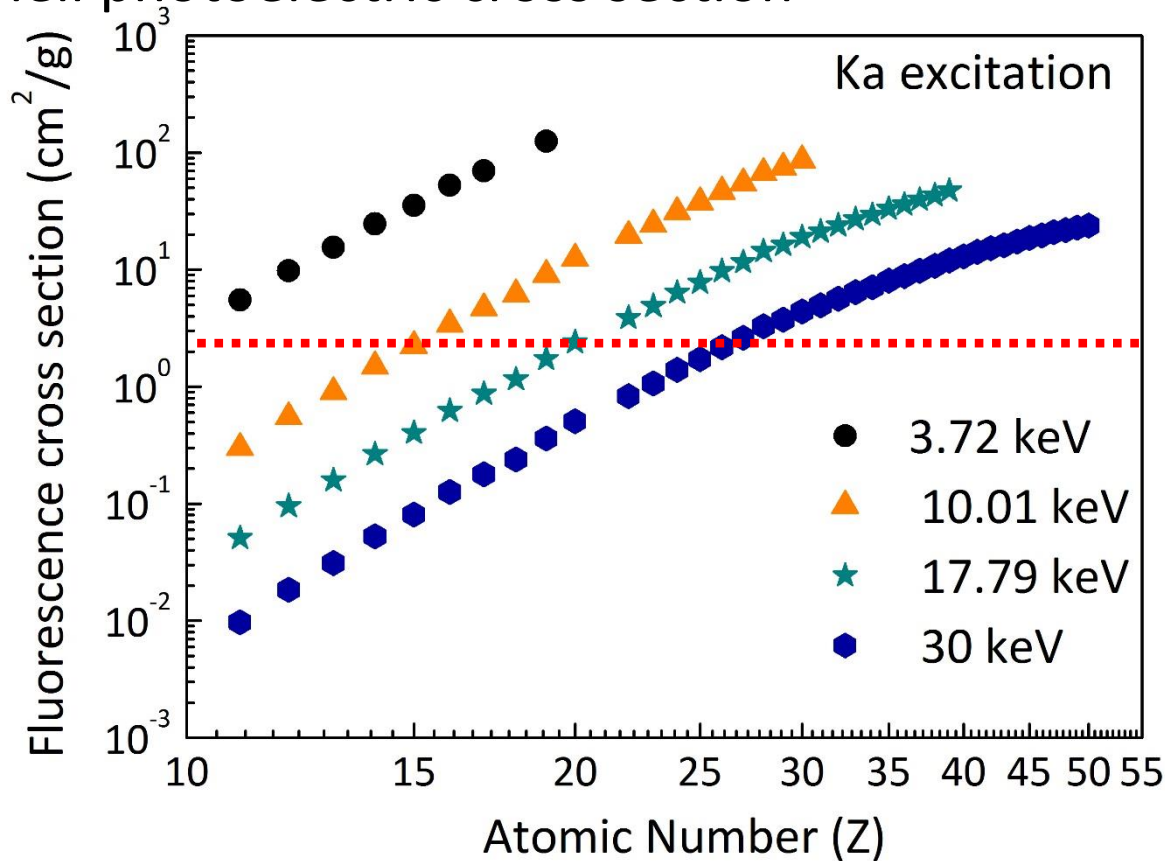
XRF K-shell fluorescence cross section  $\sigma_{KX}(E_o)$

$$\sigma_{KX}(E_o) = \tau_K(E_o) \cdot \omega_K \cdot F_{KX}$$

Transition probability for K $\alpha$  emission

K-shell fluorescence yield

K-shell photoelectric cross section

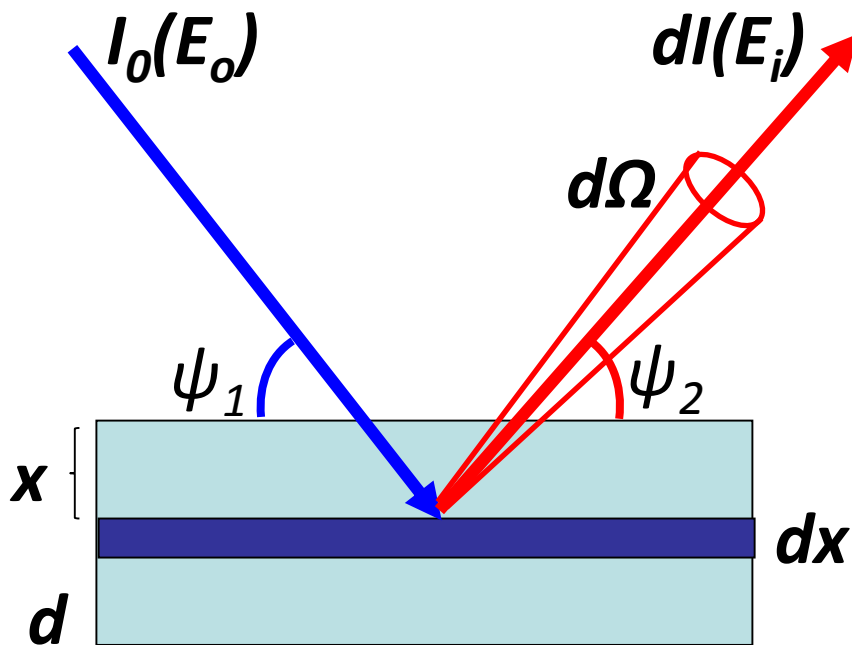


Optimizing the energy of the exciting beam for maximizing the produced characteristic X-ray intensity



# Fluorescence Emission Rate

$$dI_i(E_i) = \underbrace{I_0 \exp\left(-\frac{\mu(E_0)\rho x}{\sin \psi_1}\right)}_1 \cdot \underbrace{\frac{C_i \tau_{is}(E_0)}{\sin \psi_1} \rho dx}_2 \cdot \underbrace{\omega_{is} R_{is}(E_F)}_3 \cdot \underbrace{\exp\left(-\frac{\mu(E_i)\rho x}{\sin \psi_2}\right)}_4 \cdot \underbrace{\frac{d\Omega}{4\pi} \varepsilon_D(E_i, \Omega)}_5$$



- 1** – Rate of incident photons at depth  $x$
- 2** – Probability of production of a vacancy in the atomic shell  $s$  ( $s=K, L1, L2, L3, \dots$ ) of the element  $i$  across the path  $dx/\sin \psi_1$
- 3** – Probability of emission of a photon of energy  $E_F$  of the element  $i$  among the family of emitted photons corresponding to transitions to the atomic shell
- 4** – Transmission of the fluorescent radiation in the outgoing path towards the detector
- 5** – Overall detection efficiency for  $E_F$  photons





# Fluorescence Emission Rate: Approximation

Monochromatic excitation, Emission angle, detection efficiency constant within the solid angle

$$I_i(E_i, E_0) = I_0 C_i \omega_{is} R_{is}(E_F) \frac{\tau_{is}(E_0)}{\mu(E_0) + \mu(E_F) \frac{\sin \psi_1}{\sin \psi_2}} \left\{ 1 - \exp \left[ - \left( \frac{\mu(E_0)}{\sin \psi_1} + \frac{\mu(E_i)}{\sin \psi_2} \right) \rho d \right] \right\} \frac{\Omega}{4\pi} \varepsilon_D(E_i)$$

Thick sample:  $\rho d \gg 1$

Thin sample:  $\rho d \ll 1$

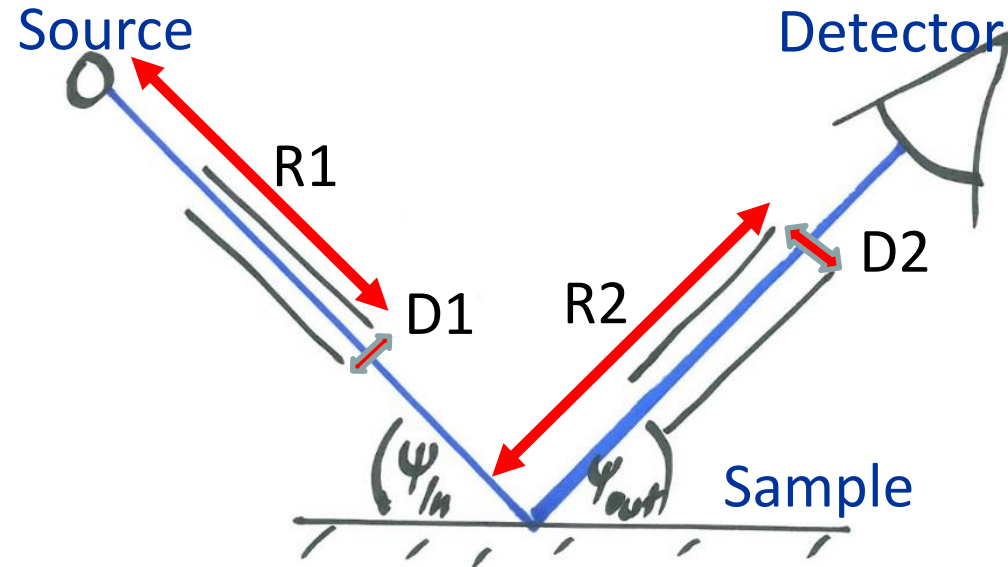
$$I_i(E_i, E_0) = \frac{I_0 C_i \omega_{is} R_{is}(E_F) \tau_{is}(E_0)}{\mu(E_0) + \mu(E_F) \frac{\sin \psi_1}{\sin \psi_2}} \left( \frac{\Omega}{4\pi} \right) \varepsilon_D(E_F) \quad I_i(E_i, E_0) = \frac{I_0 \cdot C_i \cdot R_{is}(E_f) \cdot \tau_{is}(E_0) \cdot \rho d}{\sin \psi_1} \left( \frac{\Omega}{4\pi} \right) \varepsilon_D(E_f)$$

**AND** those elements not detected also contribute to the attenuation within the whole matrix!

$$\text{Tube excitation: } I_i(E_i) = \int_{E=U_{Xi}}^{E=U_o} I(E_i, E) dE$$



# Optimization of pXRF analysis



## Fluorescence intensity depends on:

- ✓ Tube intensity, optimized spectral distribution for different elements
- ✓ Geometry:  $1/R_1^2$ ,  $D_1^2$ ,  $1/R_2^2$ ,  $D_2^2$   
 $D_2$  = diameter of detector crystal or collimator
- ✓ X-ray lens features (micro-XRF, spot size, focal distance, gain)
- ✓ Incident/outgoing sample angles
- ✓ Absorption in air paths, detector windows

## Background radiation

- ✓ Set-up geometry (scattering angle)
- ✓ Degree of exciting spectrum monochromaticity – Use of filters
- ✓ Proper collimation of exciting/fluorescence radiation to avoid parasitic lines

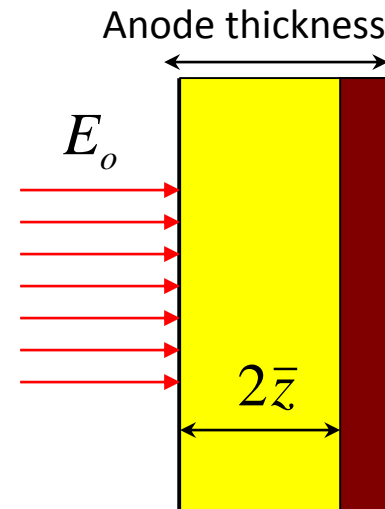
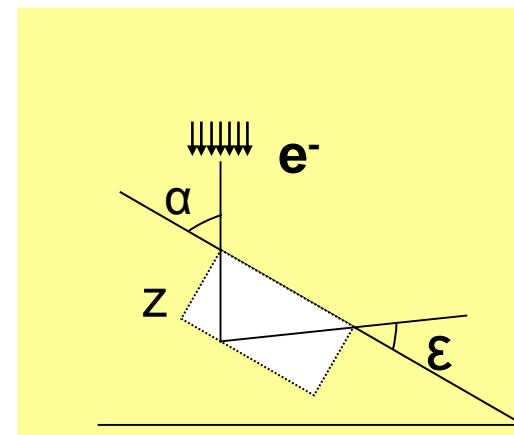


# Optimization of excitation spectrum

## X-ray tube optimization

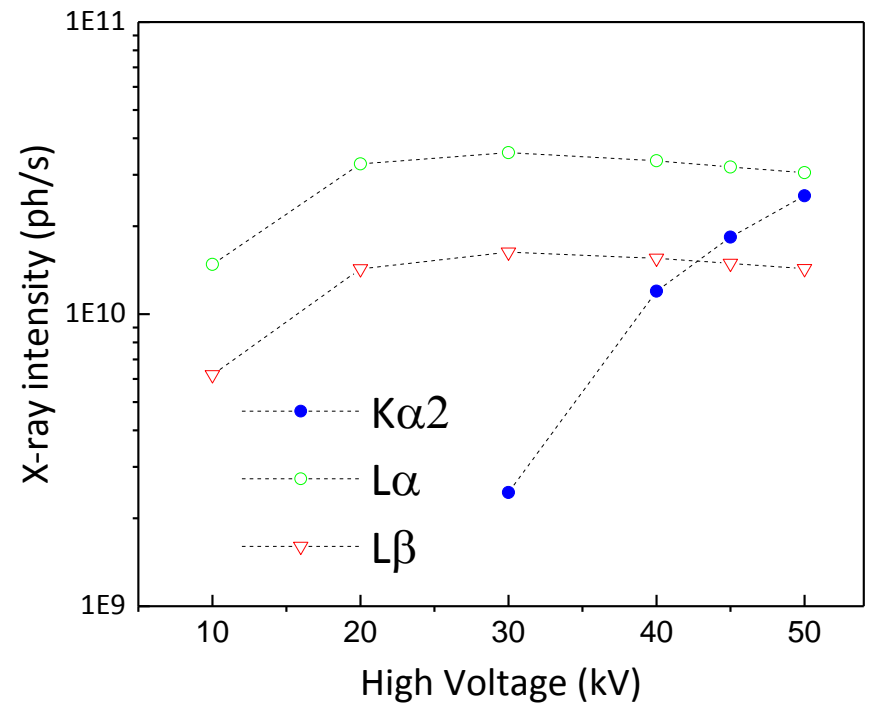
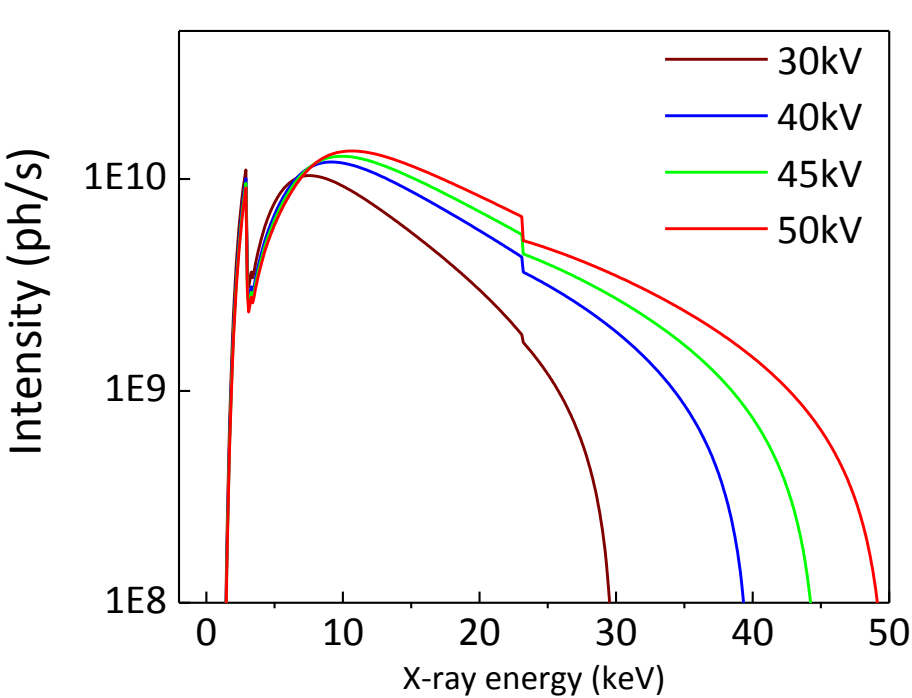
- Anode material
- High voltage
- Current
- Incident/Exit angle
- Type and thickness of tube window
- Side/End window tube
- Incident beam aperture diameter and distance

*Power consumption*





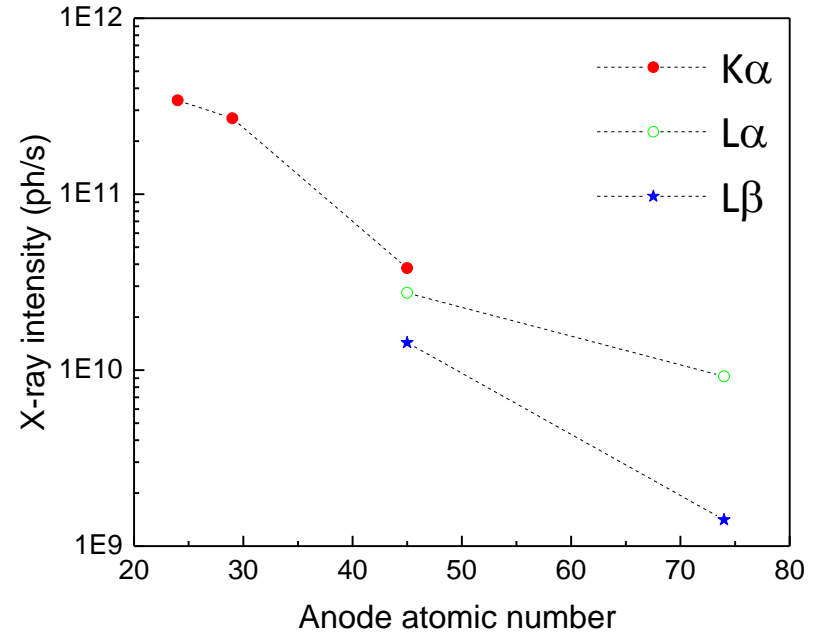
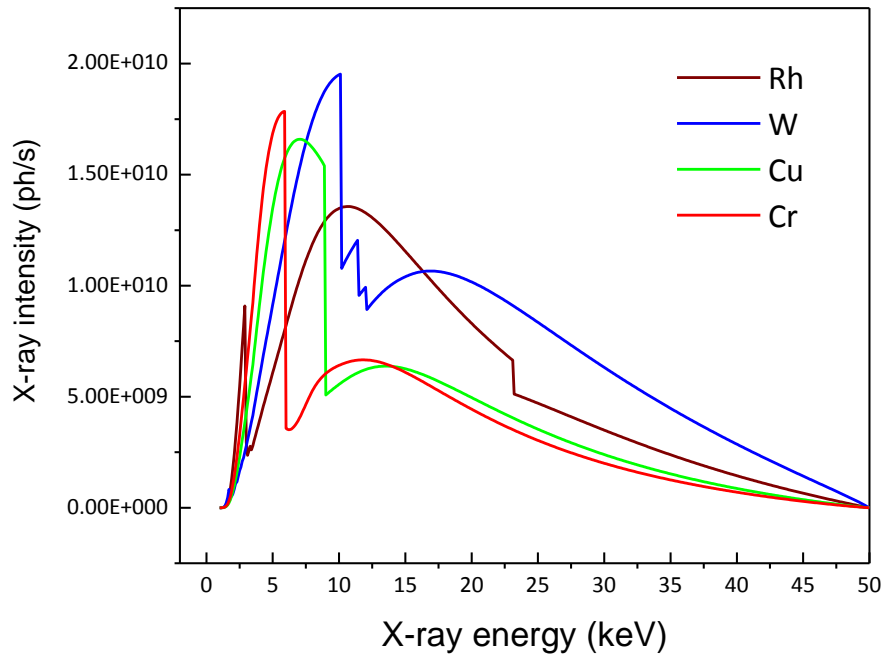
# X-ray tube optimization – High Voltage



Rh anode, 50kV, side window, standard 78/12



# X-ray tube optimization – Anode material

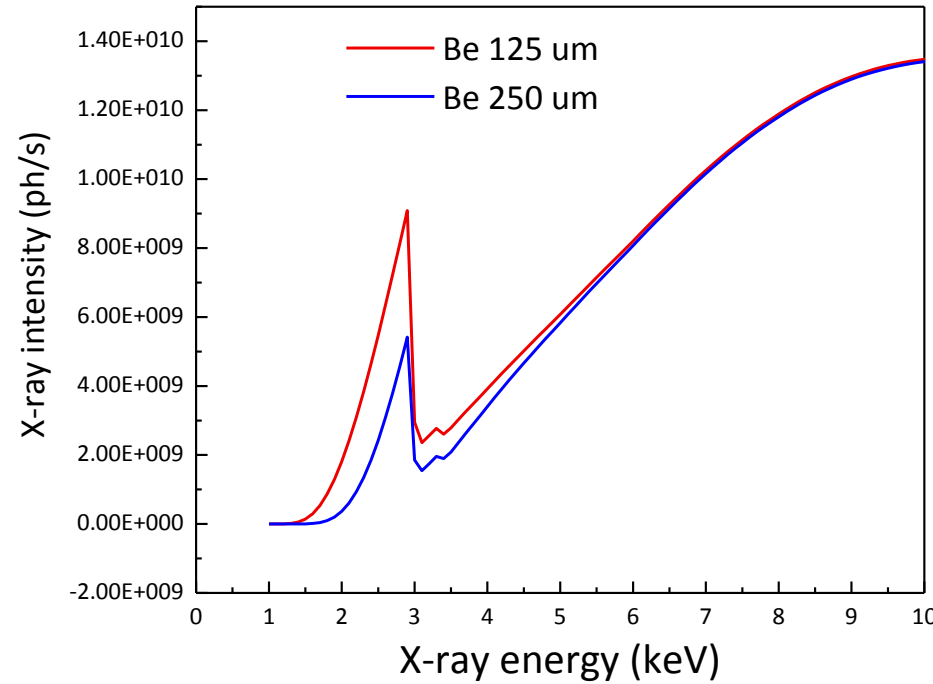
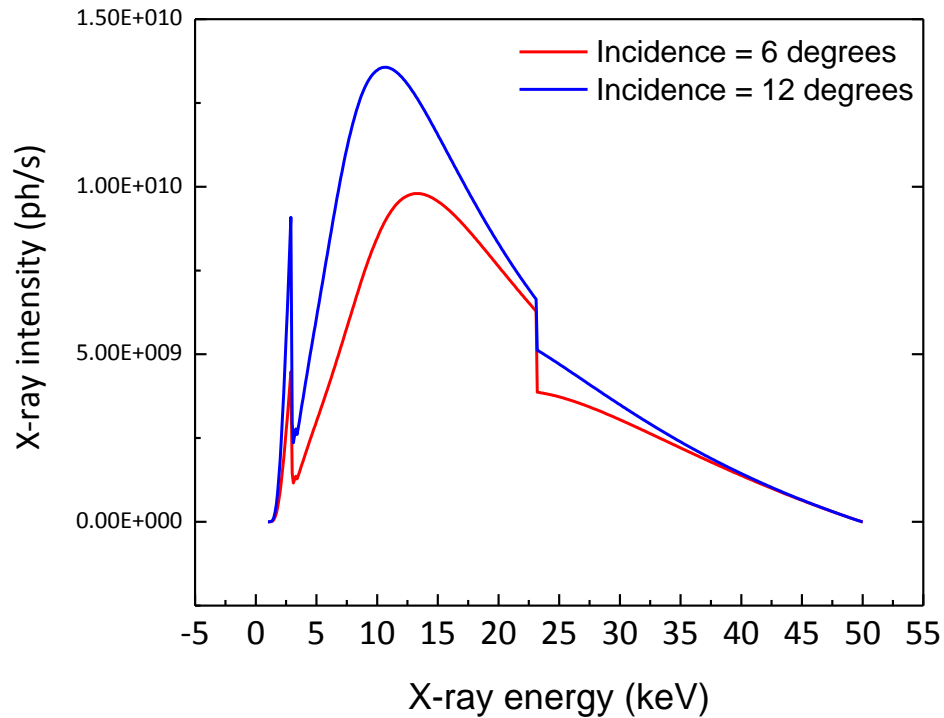


Operation at 50kV, side window



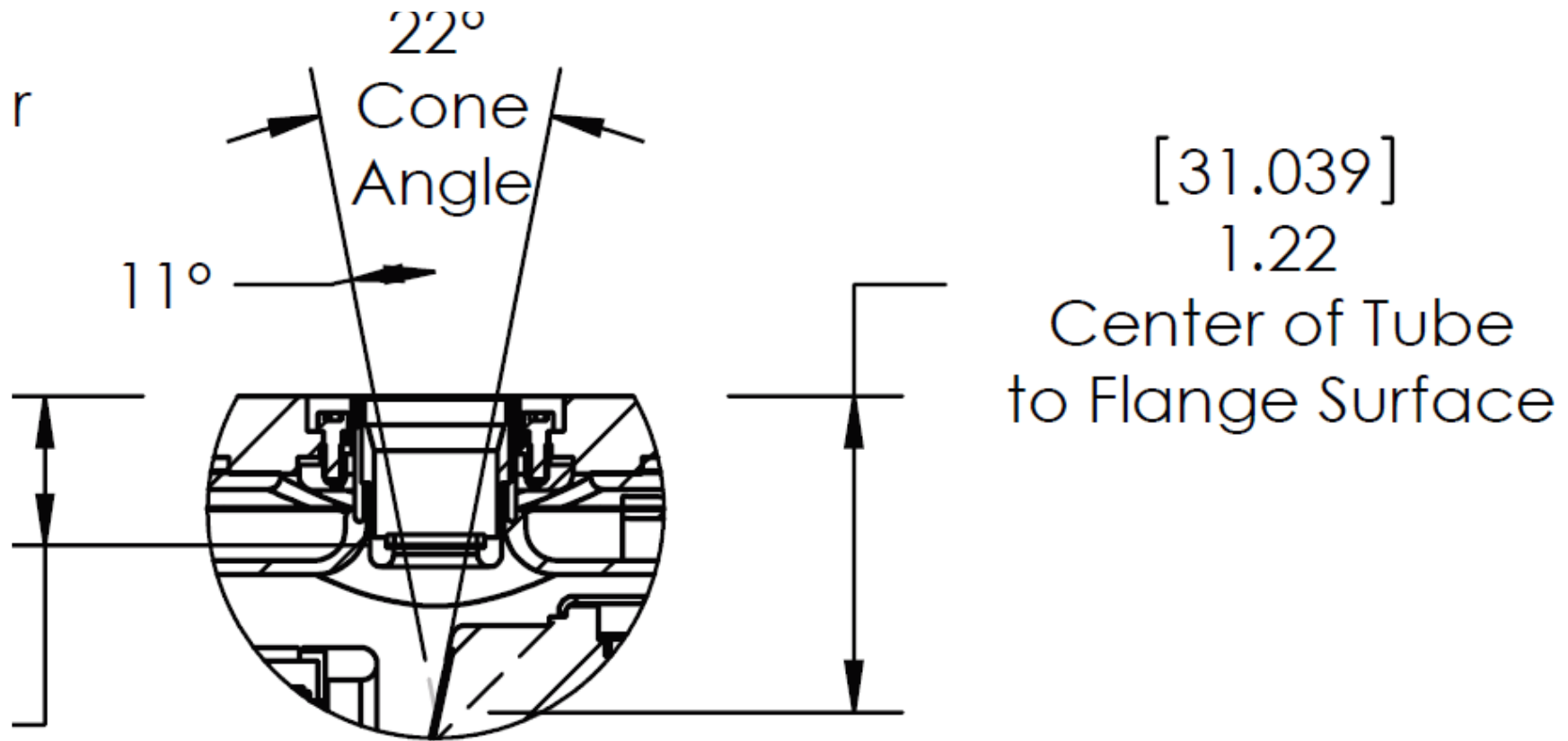
# X-ray tube – Incidence angle/Window

Rh anode, 50kV, side window





# X-ray tube geometry – Side window



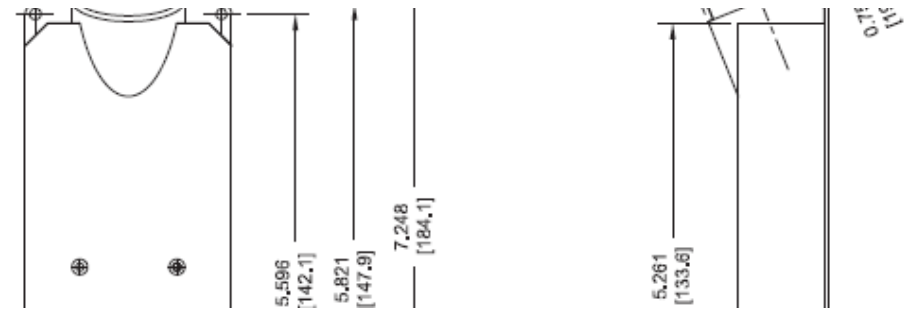
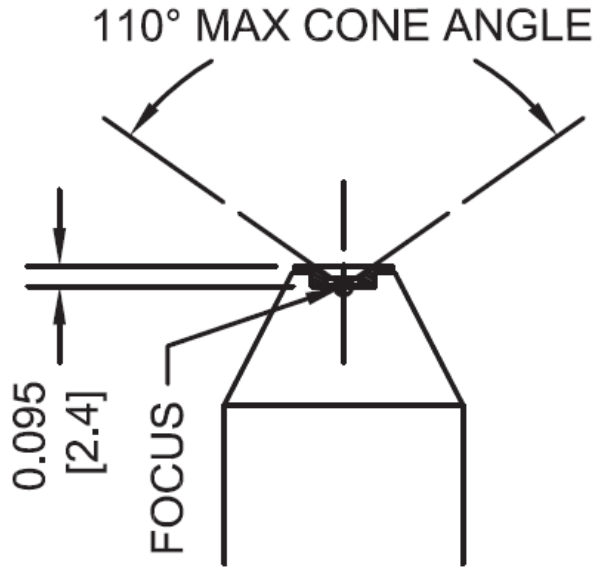
<https://xray.oxinst.com/products/x-ray-tubes/>





# X-ray tube geometry – End window

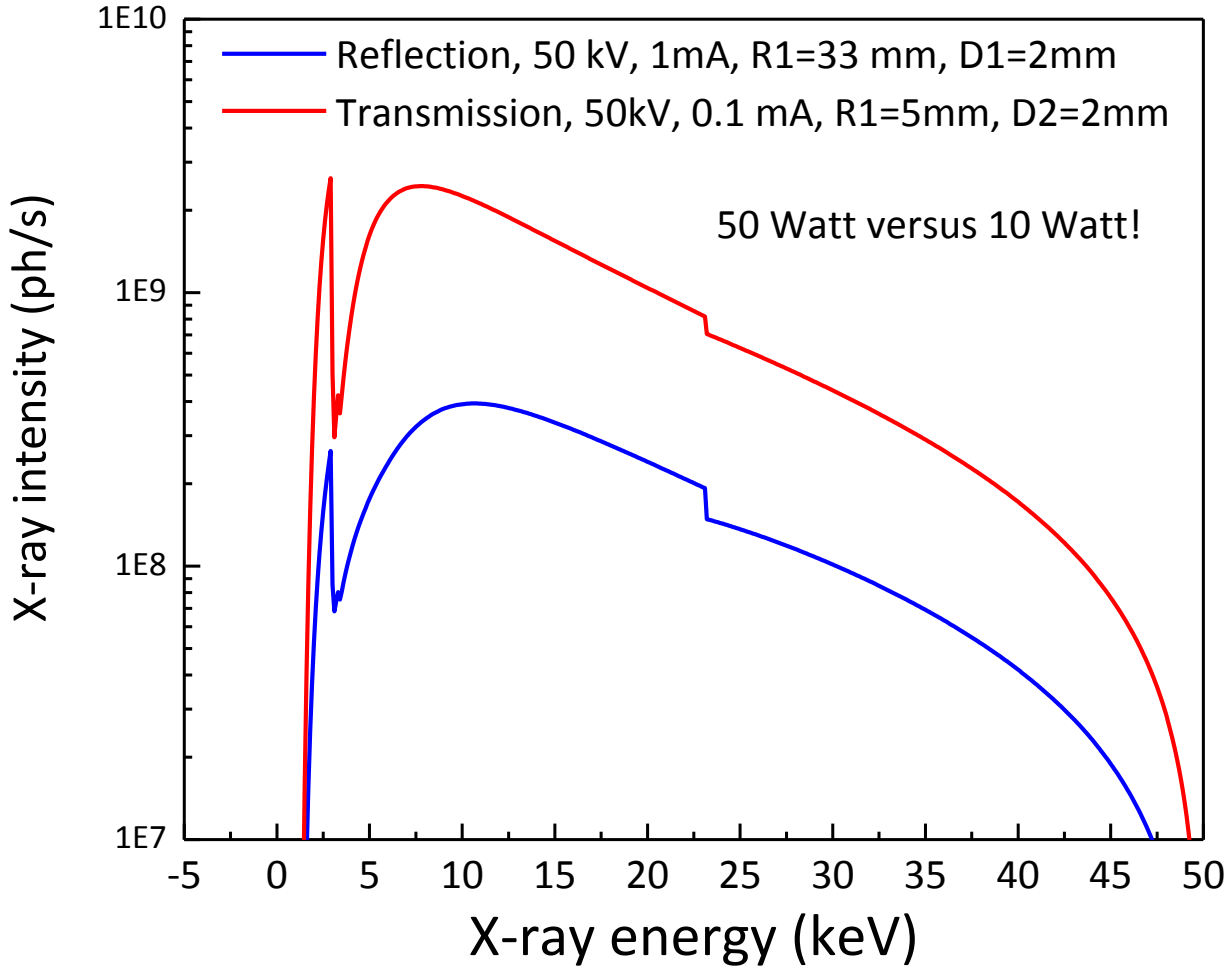
DETAIL A



<http://www.newtonscientificinc.com/>



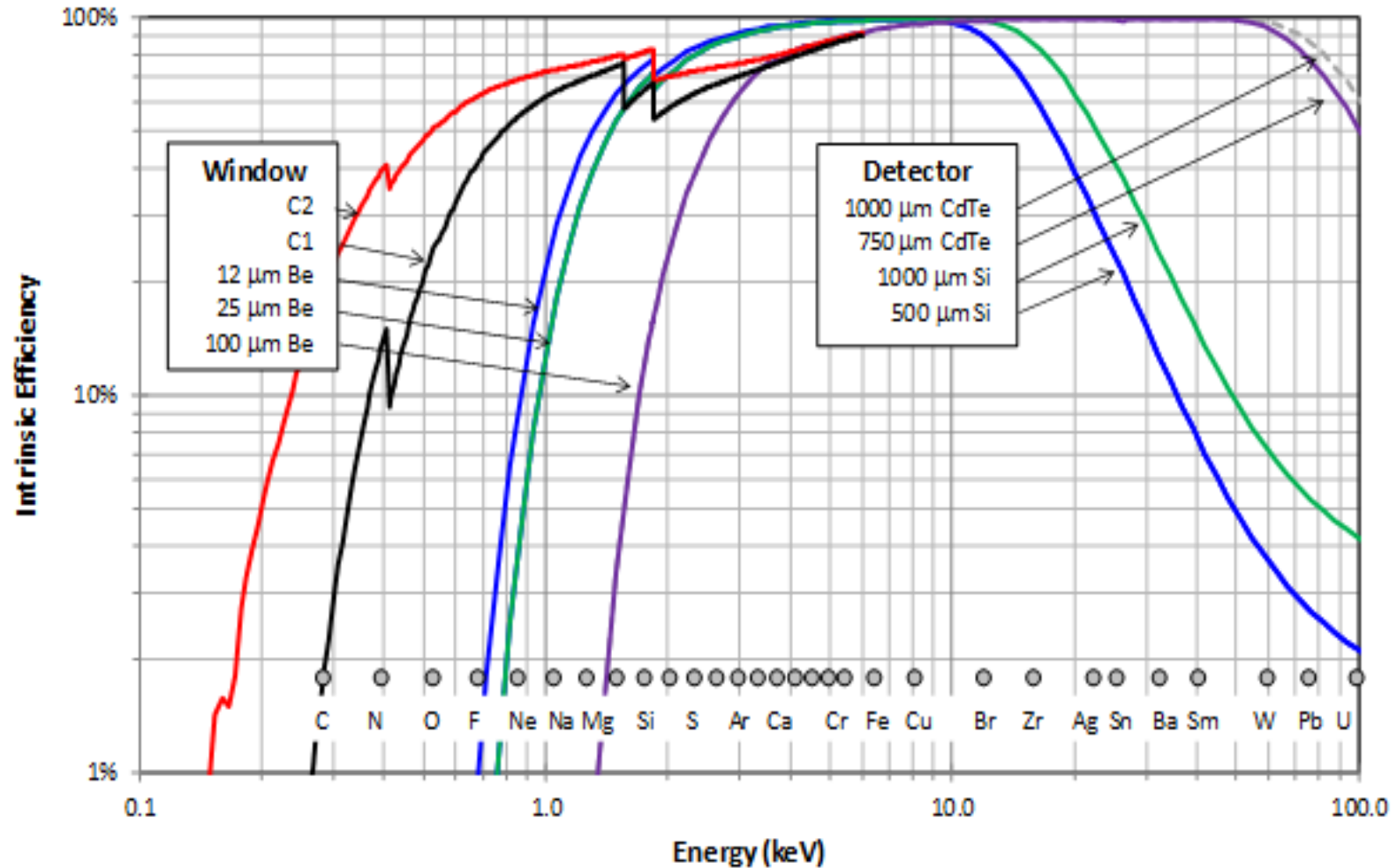
# X-ray tube geometry optimization





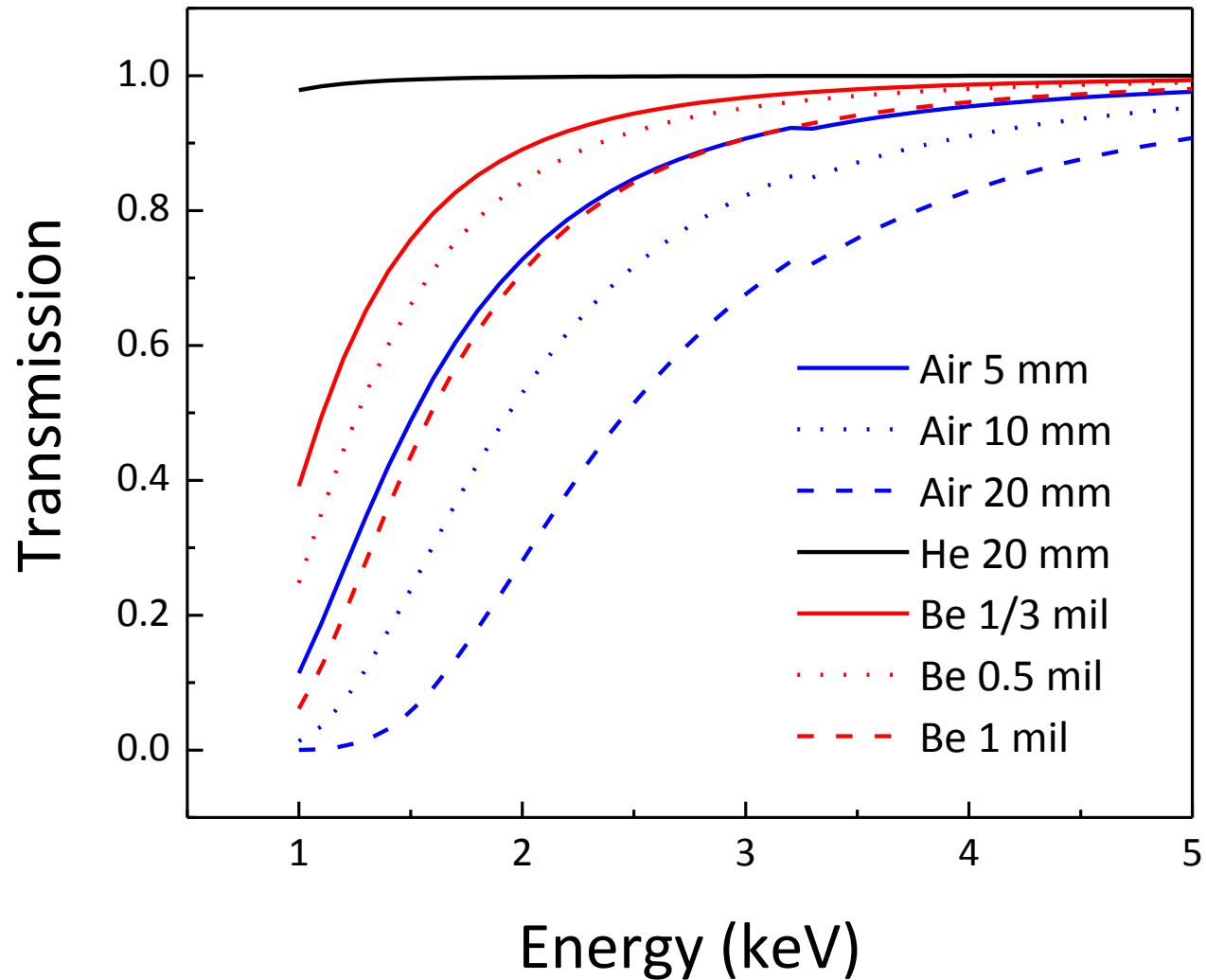
# X-ray detectors optimization:

## Window/thickness



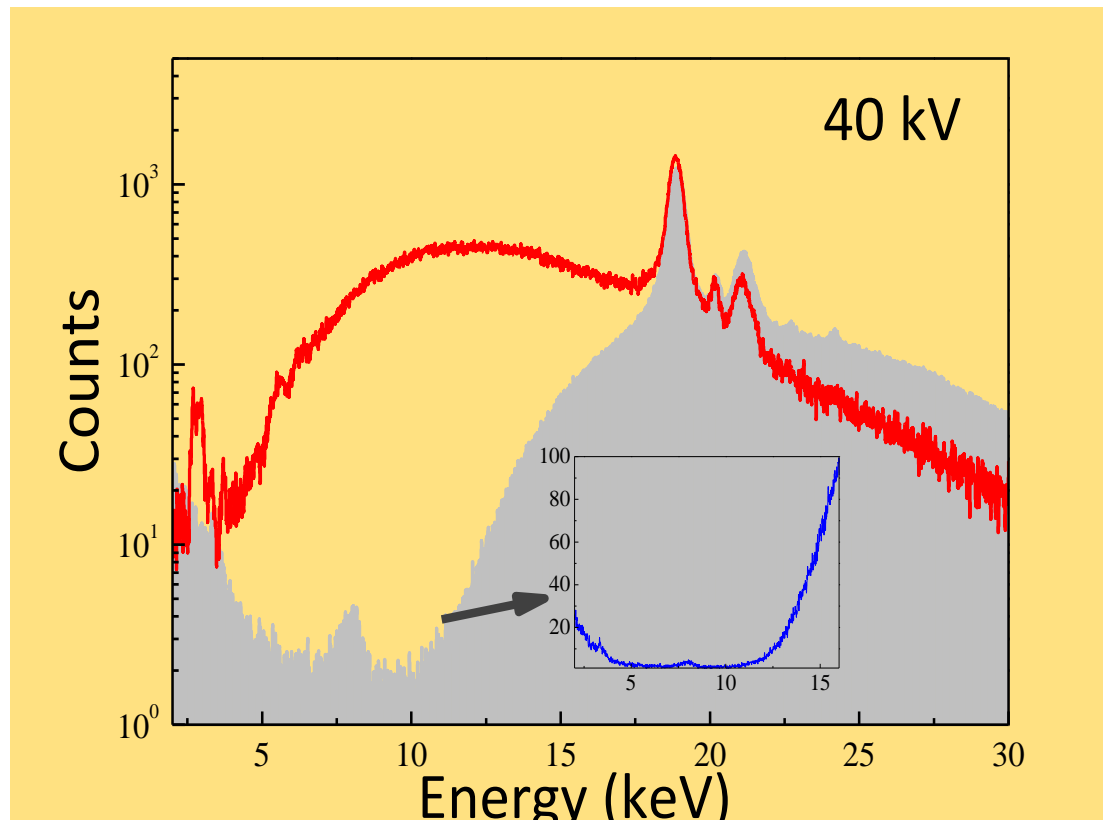


# X-ray detection environment





# Filter modifier of the exciting beam



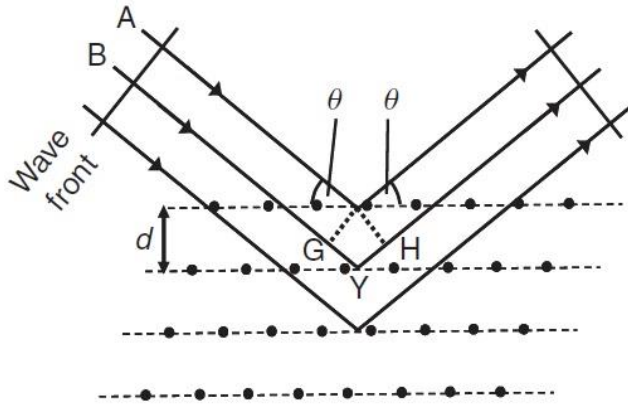
@ 19 keV: 3-4 times

@ 5-15 keV: 10-100 times



# Filtered vs Unfiltered excitation: An example

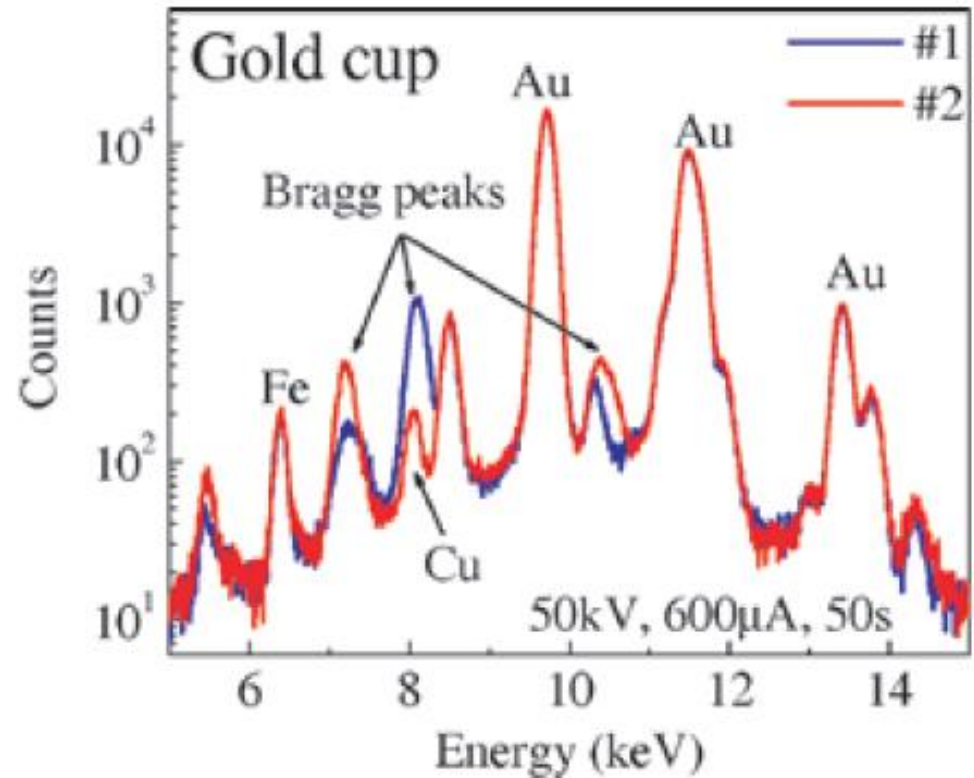
Rh anode tube, 40 kV, low atomic number scatterer



$$n\lambda = 2 \cdot d \cdot \sin \theta$$

$$E = \frac{hc}{\lambda}, E(\text{keV}) = \frac{1.2398}{\lambda(\text{nm})}$$

Bragg's Law

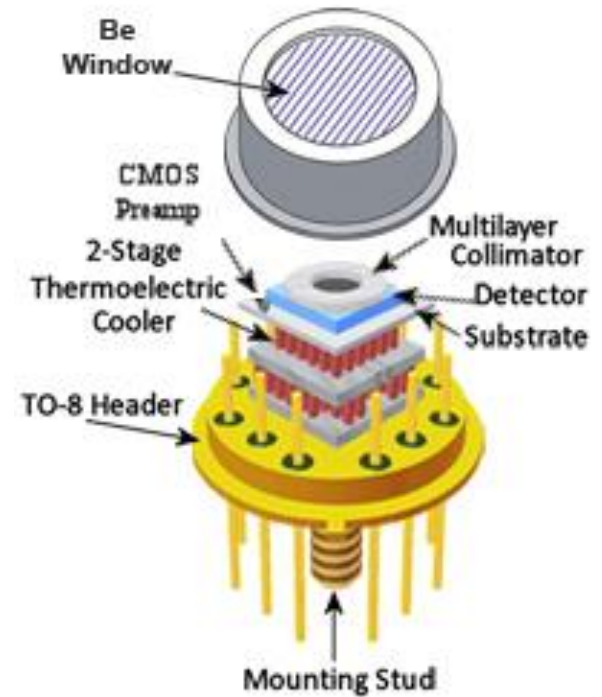




# Optimizing Det. collimation: Requirements

The detector collimation ensures:

- Detected radiation occurs only from the sample itself
- Same solid angle is defined for low and high energy fluorescent X-ray lines (Fe-K $\alpha$ , Sn-K $\alpha$ )
- Blank spectra are free of collimator material X-rays
- Elimination to certain degree of detector materials fluorescence
- Improved P/B ratio by focusing only to central area of the crystal (actual use of part of the crystal effective area)



[www.Amptek.com](http://www.Amptek.com)



**Thank you for your attention!!!**